A global map of the Zika virus phosphoproteome reveals host-driven regulation of viral budding

Inessa Manuelyan[1,2], Anna M. Schmoker[3#], Boyd L. Yount Jr.[4], Philip Eisenhauer[1], Judith I. Keller[3], Clarissa Gold[5], Dante Terino[1ǂ], Christopher M. Ziegler[1@], Jeff Alexander[6], Heather Driscoll[7], Edward Hutchinson[8], David Bhella[8], Christopher D. Syme[9], Douglas G. Widman[10¶], Mark T. Heise[10,11], Ralph S. Baric[4,10], Bryan A. Ballif[3], Jason W. Botten[1,12*]

[1]Department of Medicine, Division of Immunobiology, Robert Larner, M.D. College of Medicine, University of Vermont, Burlington, VT, USA.

[2]Cellular, Molecular, and Biomedical Sciences Graduate Program, University of Vermont, Burlington, VT, USA.

[3]Department of Biology, University of Vermont, Burlington, VT, USA

[4]Department of Epidemiology, Gillings School of Global Public Health, University of North Carolina, Chapel Hill, NC, USA.

[5]Vermont Biomedical Research Network, University of Vermont, Burlington, VT, USA.

[6]VLP Therapeutics, Inc., Gaithersburg, MD, USA

[7]Vermont Biomedical Research Network, Norwich University, Northfield, VT, USA.

[8]MRC-University of Glasgow Centre for Virus Research, University of Glasgow, Glasgow, UK.

[9]School of Chemistry, University of Glasgow, Glasgow, UK.

[10]Department of Microbiology and Immunology, School of Medicine, University of North Carolina, Chapel Hill, NC, USA.

[11]Department of Genetics, School of Medicine, University of North Carolina, Chapel Hill, NC, USA.

23 [12]Department of Microbiology and Molecular Genetics, Robert Larner, M.D. College of
24 Medicine, University of Vermont, Burlington, VT, USA.
25 [#]Current addresses: Department of Cancer Biology, Dana-Farber Cancer Institute, Longwood
26 Center, 360 Longwood Avenue, Boston, MA, USA
27 [‡]Current address: Lineberger Comprehensive Cancer Center, University of North Carolina at
28 Chapel Hill, Chapel Hill, NC, USA.
29 [@]Current address: Imanis Life Sciences, Rochester, MN, USA
30 [¶]Current address: Seqirus, Inc. 50 Hampshire Street, Cambridge, MA, USA
31
32 *Correspondence: jbotten@uvm.edu (J.W.B.); Tel.: +1-802-656-9795 (J.W.B.)
33

Abstract

Flaviviruses are enveloped, positive-strand RNA viruses that cause millions of infections in the human population annually. Although Zika virus (ZIKV) had been detected in humans as early as the 1950s, its reemergence in South America in 2015 resulted in a global health crisis. While flaviviruses encode 10 proteins that can be post-translationally modified by host enzymes, little is known regarding post-translational modifications (PTMs) of the flavivirus proteome. We used mass spectrometry to comprehensively identify host-driven PTMs on the ZIKV proteome. This approach allowed us to identify 43 PTMs across 8 ZIKV proteins, including several that are highly conserved within the *Flavivirus* genus. Notably, we found two phosphosites on the ZIKV envelope protein that are functionally important for viral propagation and appear to regulate viral budding. Additionally, we discovered 115 host kinases that interacted with ZIKV proteins and determined that Bosutinib, an FDA-approved tyrosine kinase inhibitor that targets ZIKV interacting host kinases, impairs ZIKV growth. Thus, we have defined a high-resolution map of host-driven PTMs on ZIKV proteins as well as cellular interacting kinases, uncovered a novel mechanism of host driven-regulation of ZIKV budding, and identified an FDA-approved inhibitor of ZIKV growth.

51 **Introduction**

52 ZIKV is a mosquito-borne, enveloped, positive-strand RNA virus that encodes three structural
53 proteins (capsid, C; membrane, prM; and envelope glycoprotein, E) and seven nonstructural
54 (NS) proteins (NS1, NS2A, NS2B, NS3, NS4A, NS4B, and NS5; Fig 1A). ZIKV was first
55 discovered in 1947 and confirmed as a human pathogen in 1952 (1). ZIKV belongs to the
56 *Flavivirus* genus, which has a large disease burden on the human population because of notable
57 members like dengue (DENV), West Nile (WNV), and yellow fever virus (YFV). Though
58 considered a benign disease for most of its known history, ZIKV emerged in South America in
59 2015 and resulted in a global health crisis that lasted for more than a year and caused over 1.6
60 million infections (2). Most ZIKV infections are asymptomatic, while approximately 20% of
61 those infected experience mild disease. In rarer cases, detrimental neurological complications
62 arise in the form of Guillain-Barré syndrome as well as fetal microcephaly (3, 4). Infants
63 afflicted with microcephaly because of ZIKV infection suffer developmental and health
64 consequences into childhood often with no countermeasures available; those born with severe
65 microcephaly require constant care.

66 Surveys of post-translational modifications (PTMs) on viral proteins have previously
67 been used to understand how viruses affect cells and vice versa. Viral proteins are
68 multifunctional and PTMs are an important host-driven process that can regulate viral protein
69 functionality. Discovery of PTMs can potentially elucidate novel viral protein functions. For
70 example, in human immunodeficiency virus and lymphocytic choriomeningitis virus (LCMV),
71 phosphorylation of viral proteins has been shown to be important in key processes like viral
72 particle budding and regulation of budding of different classes of viral particles (5-8). There have
73 been a small number of flavivirus phosphorylation sites discovered which demonstrate that

74 phosphorylation of viral proteins can influence the host's innate immune system or evade it,
75 affect functionality of a viral protein, impact viral protein-protein interactions, or regulate the
76 replication of viral RNA (9-13). These important discoveries emerged from studies of NS5
77 proteins of several species of flaviviruses. However, there remains an expansive terrain of other
78 flavivirus proteins. Importantly, identification of novel PTMs and their functional relevance is
79 anticipated to reveal unexplored avenues for pharmacological therapeutics in these diseases. To
80 address this gap in knowledge, herein we performed a large-scale mass spectrometry analysis of
81 the ZIKV proteome to broadly map the PTM landscape of ZIKV. Additionally, we mapped host
82 kinases that interact with the ZIKV proteome and tested whether FDA-approved inhibitors of
83 interacting kinases can be used to inhibit ZIKV growth. Finally, we functionally interrogated a
84 subset of the identified PTMs to determine their importance for ZIKV propagation and, where
85 relevant, mapped the stage of the viral life cycle impacted.
86
87 **Results**
88 ***Discovery of post-translational modifications (PTMs) on the Zika virus proteome***
89 A primary goal of this study was to identify host-driven PTMs that occur on ZIKV proteins
90 produced by mammalian cells, either in the setting of cell-free virions or within cells. Where
91 possible, we wished to examine PTMs in the setting of authentic ZIKV infection. At the time of
92 this study, the only suitable antibody available for purification of a ZIKV protein, expressed in
93 the context of an infected cell, was 4G2, which recognizes the ZIKV envelope (E) protein (14).
94 This antibody was used to purify intracellular ZIKV E and its interacting host partners from
95 infected cells (Figs 1B and 1C) or E-decorated, cell-free virions released from these same
96 infected cells (Figs 1B and 1D). Note that immunopurified ZIKV particles contained the

97 structural proteins E, prM, and C (Fig 1D and Supplementary Information 1). We also isolated
98 cell-free virions from infected mosquito cells via banding on a potassium tartrate density
99 gradient (Fig S1A). To circumvent the lack of antibodies suitable for immunoprecipitation of the
100 remaining ZIKV proteins from cells, we used plasmids to express streptavidin-binding protein
101 (SBP)-tagged ZIKV proteins. This allowed for efficient capture of SBP-tagged viral proteins via
102 magnetic streptavidin beads (Figs 1B, 1E, S2, S3, and S4). To increase the likelihood of
103 detecting phosphorylation events, transfected cells were treated with either H_2O_2, Calyculin A, or
104 DMSO to inhibit tyrosine phosphatases, serine/threonine phosphatases, or to act as a control,
105 respectively (Figs 1B, 1E, S2, S3, and S4). Samples derived from immunoprecipitation and
106 affinity purification were subjected to SDS-PAGE to orthogonally separate protein components.
107 Gel lanes were cut into multiple sections, and each piece was subjected to in-gel trypsin
108 digestion. Meanwhile, ultracentrifuged purified virus from mosquito cells (Fig S1B) was
109 digested with trypsin using filter-assisted sample preparation. All resulting tryptic peptides were
110 subjected to liquid chromatography tandem mass spectrometry for identification of PTMs or
111 interacting host proteins as described in the Methods and previously (8, 15). Tandem mass
112 spectra for discovered phosphorylation and ubiquitination sites are available in Supplementary
113 Information 2 (spectra for ZIKV E T351 from virions is available in Figs S1C, S1D).
114 We identified 18 phosphorylation sites and 5 ubiquitination sites on ZIKV E (Table 1,
115 Table S1, Figs 2A, and 2B). Two of these phosphorylation sites, Y61 and T351, were discovered
116 in the context of infection (Y61 from infected Vero E6 cells and T351 from mosquito cell-
117 derived ZIKV particles (Fig S1D). T351 was also found on ZIKV E expressed from plasmid in
118 HEK293T cells. The remaining PTMs were identified from plasmid-expressed viral proteins.
119 The locations of Y61, T351, and other PTMs found on ZIKV E are shown in Figs 2A and 2B.

120 Y61 is located in Domain II of E, which is the region responsible for dimerization (16). T351 is
121 located in Domain III, which is often a target of neutralizing antibodies (16). PTMs on E were
122 also mapped using electrostatically labeled models (Fig S5). Figure S5A shows one "face" of the
123 ZIKV E dimer as largely positively charged while Figure S5B shows the other largely negatively
124 charged face. In contrast, the border of the E dimer is mostly neutral (Fig S5C). The majority of
125 ZIKV E phosphosites were found on the neutral border of the envelope protein (Fig S5C). The
126 two phosphorylation sites on M, S16 and T18, are positioned in close proximity to one another at
127 a junction of where E and M associate (Fig 2C). Interactions between the M S16 and T18
128 phosphorylated residues with E are hard to resolve, however, because both sites are in flexible
129 regions of M and are interacting with flexible regions of E (Fig S6A).
130 We identified 11 phosphorylation sites and one ubiquitination site on NS1 (Table 1,
131 Table S1). Location mapping of PTMs on NS1 revealed that approximately half of the modified
132 amino acid residues were located in the beta-roll or beta ladder domains of NS1 (Fig 2D)
133 important for NS1 intracellular dimerization (17) and host protein interaction (18), respectively.
134 We were unable to successfully express and isolate adequate quantities of NS2A or NS3 to
135 analyze for PTMs (Fig S7). Mass spectrometry revealed a phosphorylated serine at position 71
136 on the NS2B protein (Table 1, Table S1), a small protein known to associate with NS3 to form
137 the ZIKV protease complex (Fig 2E). There were no PTMs found on NS4A despite an
138 abundance of NS4A peptides observed by mass spectrometry. One phosphorylation site was
139 detected on NS4B, though the precise location could not be determined with certainty. Our mass
140 spectrometry data suggest its location to be at either S217, S218, or T219 (Table 1, Table S1).
141 There are currently no models of ZIKV NS4B so we were unable to depict these sites within the
142 protein structure. Last, we discovered four phosphorylation sites on NS5 (Table 1, Table S1). Of

143 these, two were located in the RNA-dependent RNA polymerase region of NS5 and two in the
144 methyl-transferase region (Fig 2F).
145 To determine how conserved the discovered ZIKV protein PTMs might be with other
146 flaviviruses, we constructed a multiple sequence alignment (MSA) that included viruses
147 spanning the *Flavivirus* genus and chose flaviviruses known to cause human disease
148 (Supplementary Information 3; virus list also noted in the Methods section). In total, we
149 compared 15 different flaviviruses representing tick- or mosquito-borne viruses, viruses with no
150 known vectors, and those considered emerging pathogens. Amino acid residues were defined as
151 conserved if they were found in at least seven of the 15 flaviviruses in our panel. Of the 43
152 discovered PTMs, 14 met this degree of conservation across the *Flavivirus* genus and five were
153 conserved across nearly all flavivirus subfamilies, a result that suggests they may be
154 fundamentally important for many species of flaviviruses (Table 1). Notably, four sites were
155 found only in ZIKV isolates (Table 1).
156
157 ***Tyrosine 61 and threonine 351 on the ZIKV E protein are critical for viral growth***
158 We sought to determine whether the PTMs identified were important for viral propagation. We
159 focused on two sites, Y61 and T351 on ZIKV E, because they were found in both infection and
160 plasmid expression settings. Y61 was discovered from infected cells while T351 was found in
161 virions and on plasmid-expressed ZIKV E. Further, these sites represented residues that are
162 either highly conserved in flaviviruses (Y61) or unique to ZIKV (T351) (Table 1; Supplementary
163 Information 3). To evaluate the importance of these sites for viral propagation, we used reverse
164 genetics (19) to recover infectious ZIKV clones encoding mutations at these sites that would

165 either block or mimic phosphorylation (Fig 3A). We then used these infectious clones in multi-
166 step growth curves to determine how each change impacted viral fitness.
167 ZIKV E Y61 was mutated to a negatively-charged glutamic acid (Y61E) to reflect a
168 permanent state of phosphorylation (i.e. a phosphomimetic) and to a phenylalanine (Y61F) to
169 represent a non-phosphorylatable state. We recovered the non-phosphorylatable infectious clone
170 Y61F but, interestingly, the phosphomimetic clone Y61E appeared to be nonviable as assessed
171 by plaque assay (Fig 3B). Recovery of a Y61E clone was attempted three times without success,
172 despite successful recovery of a WT control clone each time. To account for the possibility that
173 this virus could be propagating but unable to form plaques (and therefore undetectable by plaque
174 assay), we screened for the presence of infectious virus by focus assay (Fig 3C). In parallel, to
175 account for the possibility that the virus was replicating but not with sufficient kinetics to be
176 detectable by focus or plaque assay after the initial recovery passage, we blind-passaged Y61E
177 three times. This approach led to the successful isolation of an infectious clone capable of
178 forming foci beginning at passage 3 (Fig 3C). However, sequencing of this infectious clone at
179 passage 3 revealed that the glutamic acid (Y61E) had mutated to a valine (Y61V), suggesting
180 that there is selection pressure to avoid a permanent negative charge at position 61.
181 To address whether phosphorylation of Y61 influences viral fitness, we performed a
182 multi-step growth curve comparing the phosphomutant clones Y61F and Y61V to a wild-type
183 clone. Interestingly, both the Y61F and Y61V infectious clones grew with accelerated kinetics
184 and produced higher quantities of infectious virus compared to the wild-type clone (Fig 3D;
185 Y61F $p = 0.006$).
186 ZIKV E T351 was mutated to an aspartic acid (T351D) to mimic a state of
187 phosphorylation or an alanine (T351A) to act as a non-phosphorylatable mutant. Infectious

188 clones of each mutant were successfully recovered (Fig 3B) and multi-step growth curves were
189 performed. There was no difference between the growth of the phosphomimetic T351D mutant
190 and the wild-type clone (Fig 3E; p = 0.964). Notably, the growth of the T351A non-
191 phosphorylatable mutant was impaired compared to WT virus or the T351D mutant (Fig 3E; p =
192 0.0009). After 72 hours, the titers for the T351D and the wild-type infectious clones decreased
193 more rapidly compared to T351A. This could be due to the fact that the wild-type and T351D
194 clones caused more cytopathic effect at this time point and therefore the cells could not support
195 further rounds of infection.
196 In summary, both the Y61 and T351 sites appear important for viral propagation. Our
197 results suggest that blocking phosphorylation at Y61 enhances viral growth while blocking
198 phosphorylation at T351A impairs it.
199
200 ***Y61 and T351 on ZIKV E are required for efficient Zika virus budding***
201 To determine the life cycle stage impacted by ZIKV E Y61 or T351, we next tested how a
202 phosphomimetic or non-phosphorylatable mutation at each site would impact viral budding. To
203 do so, we used a virus-like particle (VLP) assay that features a single plasmid that expresses
204 ZIKV prM and E. Once expressed, these two proteins form ZIKV VLPs that bud from cells and
205 can be detected in supernatant (20). The plasmid was mutated at ZIKV E Y61 to Y61E or Y61F
206 and at T351 to T351A or T351D. Compared to the wild-type control, VLP budding efficiency
207 was decreased when T351 was mutated to alanine (T351A) but not aspartic acid (T351D) (Fig
208 3F; p = 0.04). Mutation of Y61 to F also reduced budding efficiency (Fig 3F, p = 0.006).
209 Interestingly, we were unable to express ZIKV E protein when Y61 was mutated to Y61E
210 despite performing two bacterial transformations and evaluating several clones from each

211 transformation. This result, combined with our inability to isolate genetically stable Y61E
212 infectious clones (Fig 3C), suggests that constitutive phosphorylation at Y61 is not favorable
213 either for protein expression or viral growth. Taken together, our findings suggest that both the
214 Y61 and T351 phosphosites are required for efficient ZIKV budding.
215
216 ***Host protein kinases interact with the Zika virus proteome***
217 We next wished to determine the host kinases that associate with ZIKV proteins. The
218 immunoprecipitation and affinity purification performed in Figs 1C, 1D, 1E, S2, S3, and S4 not
219 only captured ZIKV proteins, but also their host cellular protein partners. Thus, we were able to
220 identify host kinases that interacted with ZIKV C, M, E, NS1, NS2B, NS4A, and NS4B. We
221 used Scansite 4.0 software to predict kinases that might phosphorylate ZIKV proteins at the sites
222 of phosphorylation identified in this study (Table 1). Intriguingly, some of the predicted kinases
223 were interacting partners of ZIKV proteins (Table 1, highlighted in purple). Other predicted
224 kinases, although not found by mass spectrometry to be interacting partners, either have shared
225 homology with or are found in the same cascades as interacting kinases (Table 1, highlighted in
226 blue). In total, we found 115 cellular kinases that interacted with ZIKV proteins (Table S2).
227 Figure 4A shows the top 10 most abundant kinases, determined by number of tryptic peptides
228 detected from a given viral protein during mass spectrometry. Most interacting kinases were
229 found to interact with two or more viral proteins. Five kinases interacted with 4 ZIKV proteins
230 found to have PTMs. These kinases were AURKB, CAMK2B, CDK2, PLK1, UCK2 (Aurora
231 Kinase B, Calcium/Calmodulin Dependent Protein Kinase II Beta, Cyclin-dependent kinase 2,
232 polo-like kinase 1, Uridine-Cytidine Kinase 2, respectively; Fig 4A, black circles). AURKB was

233 predicted by Scansite 4.0 to interact with ZIKV M and E, CAMK2B was predicted to interact
234 with M, and PLK1 was predicted to interact with E, NS1, NS4B, and NS5 (Table 1, Table S2).
235
236 ***Inhibition of host cell kinases by Bosutinib impairs Zika virus growth***
237 Considering that there are no FDA approved treatments for ZIKV, we next tested whether
238 selected FDA-approved kinase inhibitors might be effective in restricting ZIKV growth. We
239 focused on a panel of tyrosine and serine/threonine inhibitors to see if they could impact ZIKV
240 growth. At 10 μM, the tyrosine kinase inhibitors Bosutinib and Defactinib both reduced ZIKV
241 titers (Fig 4B; $p = 0.03$, $p = 0.02$, respectively) while Sunitinib and Imatinib did not (Fig 4B; $p =$
242 0.17, $p = 0.35$, respectively). To determine the IC_{50} of each drug, we constructed concentration-
243 response curves. To account for drug cytotoxicity, we performed simultaneous MTT assays on
244 cells that had been treated with each kinase inhibitor at the equivalent concentrations. Although
245 Defactinib inhibition of ZIKV infectious virus production reached levels as high as 86%, at the
246 same concentration of drug, cell toxicity measured 73% (Fig 4C). At Defactinib's IC_{50} of 4.5
247 μM, cell toxicity was approximately 46%. The fitted curve of inhibition and cell toxicity closely
248 followed each other, suggesting that most of the viral inhibition may have been due to nonviable
249 cells. After determining the CC_{50} of Defactinib to be 7.53 μM, we calculated the selectivity index
250 for Defactinib to be 1.7. The IC_{50} of Bosutinib was 5.5 μM. In this case, at the same doses of
251 drug, cell toxicity was approximately 17%. At higher concentrations, Bosutinib completely
252 inhibited viral growth while cell toxicity remained at approximately 30% (Fig 4D). Given
253 Bosutinib's IC_{50} and CC_{50} (17.43 μM), we calculated the selectivity index to be 3.14. These
254 results suggest that Bosutinib impairs ZIKV growth and that host cell kinases may be tractable
255 antivirals for ZIKV.

256

257 **Discussion**

258 Little is known regarding the diversity of host-driven PTMs that occur on flavivirus proteins or
259 how such modifications regulate the functionality of these proteins. We addressed this deficiency
260 by providing the first comprehensive map of phosphorylation and ubiquitination sites found on a
261 flavivirus proteome. A major finding was that selected phosphorylation sites on the ZIKV E
262 protein appear critical for ZIKV propagation, likely at the stage of viral assembly and release.
263 We also identified a network of host kinases that interact with ZIKV proteins, with many of
264 these kinases predicted to target the newly identified phosphosites. Notably, our data suggest that
265 inhibition of host kinases may be an effective approach to restrict ZIKV growth.

266 Flavivirus budding occurs at the endoplasmic reticulum and is largely driven by prM and
267 E. This pair of structural proteins together induce curvature in the ER membrane leading to the
268 formation of spherical budded virions that contain the encapsidated viral genome (21). We show
269 that the ZIKV envelope glycoprotein (ZIKV E) has at least two phosphosites, Y61 and T351,
270 which are involved in the budding stage (Fig 3F). Intriguingly, while mutation of these sites to a
271 non-phosphorylatable residue blocks efficient budding in a VLP assay (Fig 3F), infectious clones
272 of ZIKV encoding these same mutations have opposing effects – Y61F leads to enhanced
273 infectious virus production while T351A does the opposite (Figs 3D-E). To our knowledge,
274 phosphorylation of a flavivirus protein has not been implicated in the budding process. Thus, our
275 data suggests that phosphorylation of E may play a regulatory role in ZIKV budding. Moreover,
276 considering the conservation of Y61 in other pathogenic flaviviruses (Table 1, Supplementary
277 Information 3), this PTM could be fundamentally important for flavivirus budding. Additionally,
278 two ubiquitination sites on ZIKV E were recently shown to be required for viral entry and

279 replication (22). Notably, one of these ubiquitination sites, K281, was detected in the present
280 study (Table 1, Table S1).

281 Phosphosite Y61 is found in domain II of ZIKV E, the domain responsible for ZIKV E
282 dimerization (16). The inability of the phosphomimetic Y61E infectious clone to efficiently grow
283 over the first two passages following reverse genetics rescue coupled with its conversion at this
284 residue from a glutamic acid to valine by passage 3 (Fig 3C, 3D) suggest that the negatively
285 charged amino acid is not favorable. Indeed, there may be pressure at position 61 to be either a
286 non-charged or hydrophobic amino acid. A zoomed-in view of the ZIKV model reveals that Y61
287 is near an asparagine (N207) and glutamic acid (E262) (Fig S6B). In the absence of
288 phosphorylation, it is possible that the N207 and E262 residues are interacting. A large
289 phosphate group on Y61 would possibly disrupt this interaction and perhaps repel the negative
290 charge on E262, providing a possible explanation for why a non-charged state is optimal at this
291 this position. This preference is further supported by the fact that we readily rescued the
292 nonphosphorylatable mutant, Y61F, which has a hydrophobic, non-charged phenylalanine at
293 position 61.

294 The hydrophobic amino acid changes (Y to F or V) at position 61 resulted in ZIKV
295 infectious clones that outperformed wild type ZIKV in reaching peak titers (Fig 3D). We
296 interpret this finding in several ways. First, phosphorylation of ZIKV E at Y61 is either not
297 favorable to the virus or is beneficial at very specific time point(s) in the ZIKV life cycle. If the
298 latter scenario is at work, our growth curve data may not be sufficient to resolve this idea
299 because the infectious clones employed contained static mutations at this position. The
300 negatively-charged phosphosite may be important in aiding a specific purpose, such as
301 encouraging a conformational change for a period and then returning to an unphosphorylated

302 state. When mutated to Y61E, ZIKV E no longer expressed from a plasmid, suggesting that the
303 ZIKV envelope protein containing a negatively-charged glutamic acid at this position is too
304 unstable for expression or may be quickly marked for degradation. Interestingly, the Y61 site is
305 highly conserved among flaviviruses. A multiple sequence alignment (Supplementary
306 Information 3) shows that flaviviruses such as WNV, YFV, Japanese encephalitis virus (JEV),
307 and Saint Louis encephalitis virus (SLEV) also contain a tyrosine at this position, suggesting that
308 maintaining control over the charge of this tyrosine likely benefits these flaviviruses. DENV
309 contains an isoleucine at this position and more distantly related flaviviruses contain a leucine,
310 both of which share properties with tyrosine and phenylalanine in that they are also non-charged,
311 hydrophobic amino acids.

312 Another potential interpretation of Y61F and Y61E/Y61V mutations resulting in higher
313 peak infectious titers is the possibility that the phosphorylation of Y61 drives the production of
314 defective interfering particles (DIPs), but not infectious particles. Under this scenario, blocking
315 phosphorylation at Y61 would dampen the output of DIPs. The decrease in DIPs would result in
316 a greater number of permissive cells available to the infectious particles produced (i.e. more
317 replication space in the cell culture dish for infectious virions would equate to a greater
318 infectious virus output). There is a precedent for this hypothesis in our previous studies of the
319 mammarenavirus lymphocytic choriomeningitis virus (LCMV) (6, 23). In the case of LCMV,
320 phosphorylation of Y88 on the viral matrix protein - the protein that drives viral budding -
321 uniquely promotes DIP production. Y88 sits within the PPXY late domain on the LCMV matrix
322 protein. Mutation of Y88 to a nonphosphorylatable amino acid (i.e. Y88F) blocked the
323 production of DIPs and led to increased kinetics of infectious virus production. Notably, similar
324 to Y61, mutation of Y88 to a nonphosphorylatable amino acid resulted in impaired VLP

325 production (Fig 3F). This could suggest that the impairment in budding observed in both LCMV
326 Y88F and ZIKV Y61F is reflective of DI particle budding, but not infectious particles.
327 Finally, the enhanced infectious virus production observed following inhibition of Y61
328 phosphorylation could also be due to the blockage of conformational changes of ZIKV E
329 necessary for virus particle maturation. Flavivirus virion populations are composed of a mixture
330 of mature and immature virus particles. For ZIKV particles to mature, the host protease furin has
331 to cleave prM in the trans-Golgi network. This cleavage is contingent on a ZIKV E
332 conformational change that is triggered by the acidic environment of the trans-Golgi network,
333 exposing the cleavage site on prM (24). It is possible that phosphorylation of Y61 or the
334 presence of a negatively-charged amino acid at position 61 would allosterically block this
335 conformational change and shift the population of mature particles to immature particles.
336 Conversely, a lack of a negative charge at this site (i.e. Y61F or Y61V in Fig 3) may promote the
337 necessary conformational changes to occur at a higher rate, shifting the population of viral
338 particles to mature, infectious particles.
339 Phosphorylation of ZIKV E at position T351 was observed both in purified virions and in
340 cells. T351 sits within Domain III of ZIKV E, which contains motifs for cellular receptor binding
341 and is often the target of neutralizing antibodies (16). A negative charge at this position, either
342 from a phosphorylated threonine or an aspartic acid substitution, was optimal for growth (Fig
343 3E). Similarly, a negatively charged aspartic acid in the budding assay resulted in the
344 maintenance of virus-like particle budding. Conversely, mutation to an alanine, the
345 nonphosphorylatable mutant, resulted in a strong reduction in virus-like particle budding (Fig
346 3F), suggesting that host-driven phosphorylation of T351 promotes ZIKV budding. Intriguingly,
347 phosphorylation of T351 was discovered both on ZIKV E isolated from human cells as well on

348 virions derived from mosquito cells, suggesting that not only is phosphorylation of T351
349 important in the host, but that it may also play a role in the virus vector. Future studies could
350 focus on confirming the functional importance of T351 and other discovered phosphosites, such
351 as Y61, in mosquito cells, as well as evaluating whether phosphomutant viruses from mosquito
352 cells impact entry or infectivity in human cells. Because there may be differences in human and
353 arthropod kinomes, it is possible that the ZIKV phosphoproteome in vector cells would diverge
354 from our dataset in mammalian cells. Additionally, it may be that optimal viral fitness requires
355 different patterns of regulatory phosphorylation in the cells of mammalian and arthropod hosts.
356 Therefore, it would be informational to map the phosphoproteome of ZIKV in mosquito cells for
357 comparison with this dataset as well as for comparison of the roles of phosphorylation in both
358 cell types.

359 Previous studies have shown that host-driven phosphorylation of the flavivirus NS5
360 protein is critical for the flavivirus viral life cycle. For example, phosphorylation of YFV NS5 at
361 a highly conserved site (S56) is required for YFV to evade the cap-dependent innate immune
362 response in the host cell (9). Blocking the phosphorylation of another conserved flavivirus
363 residue, T449 on DENV NS5, results in a nonfunctional protein (25). Other key studies linked
364 phosphorylation of NS5 or Hepatitis C virus NS5A to important functions such as its interaction
365 with NS3 (10, 26), localization during different stages of infection (26), and viral particle
366 assembly and viral replication (11, 27). In some instances, phosphorylation of NS5 was detected
367 but not the specific residues driving the observed phenotype (10, 26). The highly conserved NS5
368 phosphosites identified in our study may be responsible for driving these important functions
369 (Table 1). Indeed, we have uncovered several highly conserved phosphosites in the ZIKV

370 proteome that may help guide the discovery of new functions for these viral proteins or the
371 mechanisms by which these functions are regulated.

372 Our mass spectrometry analysis revealed 115 host kinases (Table S2) that interacted with
373 one or more of the 8 ZIKV proteins probed, which raises the possibility that some subset of these
374 interacting kinases may be responsible for phosphorylation of these viral proteins. Treating cells
375 after infection with Bosutinib, an FDA-approved tyrosine kinase inhibitor, inhibited ZIKV
376 growth (Fig 4B-C). Indeed, a recent study by Valencia *et al.* confirmed our findings in the setting
377 of ZIKV infection in BHK-21 cells (28). One possibility is that Bosutinib is acting on CDK2, a
378 kinase found to interact with 5 ZIKV proteins (4 of which were phosphoproteins) (Fig 4A).
379 Scansite 4.0 did not predict that CDK2 would phosphorylate any of the ZIKV phosphoproteins,
380 however, host kinases can phosphorylate viral proteins at non-canonical motifs (29). Thus,
381 although not predicted, it is possible that CDK2 phosphorylates ZIKV proteins. It is also
382 important to consider that the concentration at which kinase inhibitors are administered will
383 influence their specificity; further studies are needed to identify the exact mechanism by which
384 Bosutinib decreases viral titers. Additional studies using molecules related to Bosutinib may
385 improve efficacy and specificity for blocking specific kinases. Collectively, these data imply that
386 blocking phosphorylation by host kinases is a potential antiviral strategy.

387 Several interacting kinases (ATM, ATR, and mTOR) discovered in our study were the
388 targets of early drug screens against ZIKV. Specifically, Cherry *et al*. used inhibitors VE-822
389 and WAY-600 to robustly block ZIKV infection (30). Intriguingly, VE-822 targets ATM and
390 ATR, which we found to be interacting partners of M (ATM, ATR) or E (ATM) (note that ATM
391 is predicted to phosphorylate S16 on ZIKV M; Table 1). WAY-600 targets mTOR, which we
392 found to be an interacting partner of phosphoproteins M and E as well as NS4A (Fig 4A).

393 Interestingly, mTOR was the most abundant kinase found to interact with any of the ZIKV
394 proteins (Table S2). Its importance in ZIKV was found early on when it was discovered that
395 ZIKV proteins can suppress the Akt-mTOR pathway, leading to impairment of neurogenesis and
396 upregulation of autophagy, which is beneficial for ZIKV during replication (31, 32). Another
397 study found an overall downregulation of the AKT/mTOR pathway during ZIKV infection (33).
398 Due to ZIKV M associating with high levels of mTOR (see peptide counts in Table S2), we
399 theorize that ZIKV M could be acting as a sink for mTOR, providing an explanation for why the
400 pathway is downregulated and there is less phosphorylation of mTOR targets observed during
401 ZIKV infection (33).
402 In summary, we have detailed a high-resolution map of host-driven PTMs on ZIKV
403 proteins, uncovered a novel mechanism by which ZIKV budding may be regulated, and
404 identified an FDA-approved drug that could be repurposed for the treatment of ZIKV infection.
405 The dataset described here will be useful to the field for the discovery of novel ZIKV protein
406 functions and the mechanisms by which these functions are regulated. Our work further suggests
407 that targeting host kinases may be an effective antiviral strategy and provides potential targets.
408

409 **Materials and Methods**

410 ***Cells and viruses***

411 HEK 293T/17 cells (CRL-11268), referred to as HEK293T throughout, and A549 cells (CCL-
412 185) were procured from the American Type Culture Collection (ATCC, Manassas, VA). Vero
413 E6 cells were kindly given by J. L. Whitton (The Scripps Research Institute, La Jolla, CA).
414 HEK293T cells were maintained in Dulbecco's modified Eagle medium (DMEM) containing
415 10% fetal bovine serum (FBS), 1% penicillin-streptomycin, 1% HEPES buffer solution, 1%

416 MEM nonessential amino acid solution, and 1% GlutaMAX, from Thermo Fisher Scientific
417 (Waltham, MA). A549 cells were maintained in DMEM-F12 (Thermo Fisher) containing 10%
418 FBS and 1% penicillin-streptomycin. Vero E6 cells were maintained in DMEM containing 10%
419 FBS, 1% penicillin-streptomycin, and 1% HEPES buffer solution. Cell lines described above
420 were incubated at 37°C with 5% CO_2. *Aedes albopictus* mosquito cells (C6/36; a kind gift of
421 Prof Alain Kohl, MRC-University of Glasgow Centre for Virus Research) were maintained in
422 Leibovitz's L15 media (Gibco) containing 10% FBS (Gibco), 10% triptose phosphate broth
423 (Gibco), and 1% pen/strep (Gibco) and incubated at 28ºC. ZIKV strain BeH819015, a Brazilian
424 isolate (GenBank: KU365778.1), was generously provided by the Baric Lab (University of North
425 Carolina, Chapel Hill, North Carolina, USA) (19). The Zika virus strain used to infect mosquito
426 cells was ZIKV/H.sapiens/Brazil/PE243/2015 (Recife, Brazil) (34). Working stocks of infectious
427 ZIKV, including recombinant ZIKV clones generated via reverse genetics (see below for details
428 on recovery), were grown on Vero E6 cells and titered by standard plaque assay.

429 ***Plasmids***

430 Several plasmids were used for expression of ZIKV proteins. The nucleotide sequences of ZIKV
431 ORFs used in this study were derived from ZIKV strain H/PF/2013 (NCBI gene identifier
432 number AHZ13508). The Heise lab (University of North Carolina, Chapel Hill, North Carolina,
433 USA) provided their pOME plasmid-based library that permits expression of each ZIKV ORF
434 containing a C-terminal 3XFLAG tag (35). To enable streptavidin-based affinity purification of
435 ZIKV proteins, the ZIKV C, E, M, NS1, NS2B, and NS4A ORFs encoded in the pOME plasmids
436 were subcloned into our modified pCAGGS expression vector (36, 37) such that they would
437 encode a C-terminal streptavidin binding peptide (SBP)
438 (MDEKTTGWRGGHVVEGLAGELEQLRARLEHHPQGQREP) in place of the 3XFLAG tag.

439 Each ZIKV ORF was fused to the SBP tag through an 18 base pair linker. The nucleotide
440 sequence of the ZIKV genes was amplified by PCR from the pOME vectors with forward
441 primers that contained a 5' overhang containing a Gateway AttB1 site and a Kozak sequence and
442 reverse primers containing an overhang with the linker sequence (all primers used are listed in
443 Supplementary Information 4). The SBP tag was amplified from a previously generated in-house
444 plasmid via PCR using the forward primer SBP (5'-
445 GCAGCTGGAGGTGGAGGTATGGACGAAAAAACCACCGGT-3'), which has a 5' overhang
446 containing the linker sequence, and the reverse primer SBP (5'-
447 ACCACTTTGTACAAGAAAGCTGGGTCTTACGGTTCACGCTGACCCTGCGG-3'), which
448 contains a 3' overhang with a stop codon preceding an AttB2 sequence. The two PCR products
449 (each respective amplified ZIKV gene and the amplified SBP tag) were fused by PCR using the
450 appropriate ZIKV gene forward primer and the SBP reverse primer. The resulting cassette was
451 subcloned into the modified pCAGGS vector using the Gateway cloning system (Invitrogen)
452 following the manufacturer's instructions. pOME plasmids encoding ZIKV NS2A, NS3, NS4B,
453 or NS5, each with the same C-terminal linker and SBP tag as described directly above, were
454 generated by GenScript Biotech Corporation (Piscataway, NJ, USA) but were maintained in the
455 original pOME vector. Plasmids for the ZIKV reverse genetics system were kindly provide by
456 the Baric Lab as described in Widman *et al.* (19). The plasmid from the Baric system which
457 contained the ZIKV E gene was modified by GenScript to include the Y61F, Y61E, T351A, and
458 T351D mutations. The plasmid used for the virus-like-particle budding assay, which encodes the
459 ZIKV prM and E genes, is described here (20) and was generously provided by Emergent
460 BioSolutions, Inc. This plasmid was also modified by GenScript to include the include the Y61F,
461 Y61E, T351A, and T351D mutations. All plasmid sequences were verified by DNA sequencing.

462 ***Identification of post-translational modifications of ZIKV proteins by mass spectrometry***

463 To identify phosphorylation sites on ZIKV proteins via mass spectrometry, three general
464 approaches were taken. In the first approach, to purify ZIKV E, Vero E6 cells were infected with
465 ZIKV at an MOI of 0.1 and 72 hours later cells were collected, and lysed in Triton buffer
466 consisting of 1% Triton X-100, 0.5% NP40, 140mM NaCl, and 25mM Tris-HCl containing a
467 protease inhibitor cocktail (04693159001, Roche Applied Science, Indianapolis, IN) as well as
468 PhosStop phosphatase inhibitor cocktail (04906837001, Roche Applied Science). The resulting
469 protein lysate was incubated with anti-ZIKV E 4G2 antibody at 4°C, overnight. The next day,
470 magnetic Protein G Dynabeads (ThermoFisher Scientific, Waltham, MA) were added to the
471 lysate-antibody mixture and incubated at 4°C, rotating for at least 4 hours (but not more than 8
472 hr). Beads were then magnetically isolated, gently washed 3 times in Triton buffer, magnetically
473 isolated for a final time and then boiled in Laemmli buffer (62.5 mM Tris-HCl, 10% glycerol,
474 2% sodium dodecyl sulfate and 0.01% bromophenol blue (B392, Fisher Scientific, Pittsburgh,
475 PA) for 5 minutes to release antibody, ZIKV E protein, and associated host or viral protein
476 partners. Similarly, ZIKV virions were immunopurified from infected Vero E6 cell media 96
477 hours post-infection using Dynabeads coated with anti-ZIKV E 4G2 antibody then lysed using
478 10X Triton buffer containing the same protease and phosphatase inhibitor cocktails described
479 directly above.

480 To purify ZIKV proteins expressed from plasmid, our second approach was to transfect
481 HEK293T cells with modified pCAGGS plasmid expressing ZIKV C, M, E, NS1, NS2B, NS4A,
482 NS4B, or NS5 proteins with a C-terminal SBP tag in each case. $5x10^5$ cells per well in 6-well
483 plates were transfected with 2 µg of plasmid using 8 µg of polyethylenimine (23966,
484 Polysciences, Inc., Warrington, PA), which was reconstituted at 1 mg/mL. Two days later,

485 transfected cells were treated either with DMSO (D2650, Sigma-Aldrich. Saint Louis, MO),
486 H_2O_2, (Thermo Fisher) or Calyculin A (Cell Signaling Technology, Danver, MA) for 20 minutes.
487 Cells were collected and lysed with Triton buffer (same formulation described above) and then
488 subjected to affinity purification using magnetic MyOne Streptavidin T1 beads (65601, Thermo
489 Fisher Scientific) according to the manufacturer's instructions. Briefly, magnetic beads were
490 washed in buffer several times, added to protein lysates from transfected cells, and then rotated
491 overnight at 4°C. The next day, the beads were magnetically isolated and washed several times
492 with lysis buffer containing protease and phosphatase inhibitors and then boiled in Laemmli
493 buffer for 5 minutes to release SBP-tagged ZIKV proteins from the streptavidin beads.
494 Infected cell lysates, transfected cell lysates, and virion protein lysates were separated on
495 4-20% Tris-Glycine polyacrylamide gels (EC60255, Invitrogen). To visualize protein bands for
496 excising and mass spectrometry processing, gels were stained with Coomassie (40% methanol,
497 20% acetic acid, and 0.1% Brilliant Blue R (B7920, Sigma-Aldrich)). Gels were destained with a
498 solution of 30% methanol and 10% acetic acid and imaged using a Canon Canoscan 8800F
499 scanner. Sample lanes were cut into a series of gel pieces containing prominent protein bands or
500 band groups. After excision, gel pieces were further cut into 1 mm cubes and processed.
501 Chemicals used for processing were purchased from Thermo Fisher Scientific. Gel pieces were
502 rinsed with HPLC-grade water and then incubated with destain solution (50 mM ammonium
503 bicarbonate and 50% acetonitrile) for 30 minutes at 37°C. Destain was removed and gel pieces
504 were dehydrated by incubating twice with 100% acetonitrile for 5 minutes. The gel pieces were
505 reduced with 25 mM dithiothreitol in 50 mM ammonium bicarbonate for 30 minutes at 55°C.
506 After cooling, gel pieces were dehydrated with 100% acetonitrile for 5 minutes and then
507 alkylated with 10 mM iodoacetamide in 50 mM ammonium biocarbonate for 45 minutes at room

508 temperature, while protected from light. Gel pieces were washed twice in destain solution for 5
509 minutes, dehydrated with 100% acetonitrile, then rehydrated with water for 10 minutes. Gel
510 pieces were further dehydrated with two 5-minute incubations in 100% acetonitrile. All liquid
511 was removed and gel pieces were left to incubate at room temperature to evaporate trace
512 acetonitrile. Gel pieces were rehydrated with a solution of 12.5 ng/µL sequencing-grade,
513 modified trypsin (V5111, Promega) in 50 mM ammonium bicarbonate on ice for 30 minutes,
514 before digesting overnight at 37°C. Peptides were extracted with a solution of 2.5% formic acid
515 in 50% acetonitrile while spinning in a microcentrifuge at 13,000 rpm for 10 minutes. The
516 supernatant was removed and saved while the gel pieces were subjected to further extraction and
517 rinsing with 100% acetonitrile. The second extraction was combined with the initial extraction.
518 All solvent was removed from the extracts using a vacuum centrifuge at 37°C. The peptides were
519 resuspended in 2.5% formic acid, 2.5% acetonitrile prior to mass spectrometry analysis.
520 Dried peptides were resuspended in Solvent A (2.5% MeCN, 0.15% formic acid (FA)) and
521 separated using the Easy n-LC 1200 across 15-cm columns packed in-house with 2.7 µm C18
522 packing material prior to analysis on the Q Exactive Plus mass spectrometer fitted with a
523 Nanospray Flex ion source (2.2 kV) and supplied with Thermo Xcalibur 4.0 software. Peptides
524 were eluted using a 0 - 50% gradient of Solvent B (80% MeCN, 0.15% FA) over 60 min,
525 followed by 10 minutes at 95% Solvent B. The precursor scan (scan range = 360–1700 *m/z*,
526 resolution = 7.0 x 10^4, maximum IT = 100 ms) was followed by HCD fragmentation spectra in a
527 Top-10 approach (resolution = 3.5 x 10^4, AGC = 5.0 x 10^4, maximum IT = 50 ms, isolation
528 window = 61.6 *m/z*, normalized collision energy = 26%, dynamic exclusion = 30 s). Raw spectra
529 were searched against a forward and reverse database of tagged ZIKV proteins with common
530 contaminants added using SEQUEST with a precursor mass tolerance of ± 5 PPM and a

531 fragment ion tolerance of ± 0.006 Da. The following differential modifications were permitted:
532 phosphorylation of serine, threonine and tyrosine (±79.9663 Da), ubiquitylation of lysine
533 (±114.0429 Da), oxidation of methionine (±15.9949 Da), carboxyamidomethylation of cysteine
534 (±57.0215 Da), and acrylamidation of cysteine (±71.0371 Da). No enzyme was indicated in the
535 original search to expand the database, and the resulting hits were filtered for tryptic peptides.
536 Spectra of phosphopeptide hits were manually assessed and compared to their unphosphorylated
537 counterparts to confirm hits and determine phosphorylation site localization. To identify bound
538 human interactors, raw data were searched against a forward and reverse human database
539 containing common contaminants via SEQUEST. Trypsin was specified as the cleavage agent
540 with two missed cleavages permitted. Mass tolerances and allowed modifications were as stated
541 above. Host proteins were considered ZIKV interactors if they were identified by two or more
542 unique peptides in experimental conditions and were not present in the controls. Proteins were
543 also considered ZIKV interactors in cases where proteins were >5-fold enriched in experimental
544 over control conditions.

545 In our third approach, which led to the identification of ZIKV E T351 from virions,
546 C6/36 cells were infected with ZIKV at an MOI of 0.1 and then incubated at 28ºC. Four days
547 later, the supernatant was harvested and clarified by centrifugation at 5000 rpm. The clarified
548 supernatant was concentrated using 100,000 MW cut-off Centricon concentrators (Millipore).
549 The concentrate was underlayed with a 5 mL sucrose cushion (24% w/v in 1x NTE buffer; NaCl-
550 Tris-EDTA) and ultracentrifuged at 105,000 *g* in a Surespin 630 Rotor (Thermo Scientific) for
551 1.5 hours. The pellet-associated virus was resuspended in NTE, then overlaid onto a 10-35%
552 (w/v) / density gradient of potassium tartrate in 30% glycerol in NTE, prepared using a Gradient
553 Master (Biocomp Instruments). Virions were banded by ultracentrifugation at 175,000 *g*

554 overnight and collected by pipetting from the top of the gradient. Next, the virus-containing
555 fraction was removed from the gradient, placed in 100,000 MW cut-off dialysis units, and
556 dialyzed several times using 1× NTE to remove the potassium tartrate and glycerol. After
557 dialyzing overnight, virus was concentrated using 100,000 MW cut-off Centricon concentrators
558 (Millipore).

559 Concentrated ZIKV virions were inactivated at 70°C in 4M final urea in TEAB and then
560 prepared for liquid chromatography and tandem mass spectrometry (LC-MS/MS) as described
561 (38). Briefly, the sample was reduced, alkylated, and then digested with trypsin and LysC using
562 filter-assisted sample preparation (FASP) (39). Peptides were separated by reversed-phase
563 chromatography using a 2h gradient on an Ultimate 3000 RSLCnano HPLC system (Dionex).
564 This was run in direct injection mode and coupled to a Q Exactive mass spectrometer (Thermo),
565 running in 'Top 10′ data-dependent acquisition mode with fragmentation by higher-energy
566 collisional dissociation (HCD). Charge state + 1 ions were rejected and fragmentation and
567 dynamic exclusion with 40 s was enabled. Mass spectra were annotated in MaxQuant version
568 1.6.3.4 (40) with reference proteomes from Zika virus isolate
569 ZIKV/H.sapiens/Brazil/PE243/2015 (GenBank KX197192.1) and *Aedes aegypti* (UniProt
570 UP000008820, accessed on 2018-10-26) and the MaxQuant common contaminants list. Standard
571 settings were used, with the enzyme set as trypsin/P and fixed modifications set as
572 carbamidomethyl (C). Variable modifications were oxidation (M), acetyl (Protein N-ter),
573 phospho (STY) and, to account for artefactual modifications when inactivating in urea, carbamyl
574 (KRC). Modified spectra were considered where they could be identified in the absence of
575 artefactual carbamylation. Data from this third approach can be found at
576 https://researchdata.gla.ac.uk/1222/.

577 ***Multiple sequence alignment***

578 A multiple sequence alignment (MSA) of flavivirus FASTA-formatted sequences was generated
579 using the MUSCLE (Multiple Sequence Comparison by Log-Expectation) algorithm (41) as
580 implemented in the NIAID Virus Pathogen Database and Analysis Resource (ViPR) through the
581 web site at http://www.viprbrc.org/ (42). The Uclust parameter was set as a MUSCLE pre-
582 processor to improve both speed and quality of alignment. The alignment visualization with
583 PTM annotations was created in Jalview 2.11.1.4 (43). The following flaviviruses were aligned:
584 ZIKV H/PF/2013 (AHZ13508), ZIKV Uganda (ABI54475), ZIKV SPH2015 (ALU33341),
585 ZIKV Paraiba (ANH10698), ZIKV USA UT (AOO19564), ZIKV BeH819015 (AMA12085),
586 DENV 1 NP059433), DENV 2 (NP056776), DENV 3 (YP001621843), DENV 4 (NP073286),
587 JEV (Japanese encephalitis virus; NP059434), SLEV (Saint Louis Encephalitis Virus;
588 YP001008348), USUV (Usutu virus; AAS59401), WNV 1(YP001527877), WNV 2
589 (NP041724), AHFV (Alkhurma hemorrhagic fever virus; AAL08421), KFDV (Kyasanur forest
590 disease virus, AAQ91607), OHFV (Omsk hemorrhagic fever virus, AAQ91606), TBEV (tick-
591 borne encephalitis virus; NP043135), ENTV (Entebbe bat virus; AAV34153), MMLV (Montana
592 myotis leukoencephalitis virus, CAC82713), LAMV (Lammi virus, ACR56717), YFV
593 (NP041726), and PCV (Palm Creek virus, AGG76014).

594 ***SDS-PAGE and western blotting***

595 Protein lysates were diluted in Laemmli buffer, boiled for 5 minutes, then separated on NuPAGE
596 4–12% Bis-Tris gels with MES buffer. Protein was transferred to nitrocellulose membranes
597 using iBlot gel transfer stacks (IB301001 or IB301002, Invitrogen) and the Invitrogen iBlot
598 Device according to manufacturer instructions. Membranes were blocked with 5% milk in PBS
599 for 1 hour and incubated overnight with primary antibody diluted in PBS which contained 5%

600 milk and 0.2% Tween 20 (BP337, Fisher Scientific). The following day the membrane was
601 rinsed several times with TBST (tris-buffered saline with 0.1% Tween 20) then incubated for 1
602 hour with secondary antibody diluted in PBS containing 5% milk, 0.2% Tween 20, and 0.02%
603 SDS. After secondary antibody incubation, the membrane was washed several times in TBST
604 then washed in PBS before imaging on a LI-COR Odyssey CLx system.

605 Primary antibodies were used for western blotting at the following concentrations: mouse
606 anti-ZIKV E (4G2) (1:10,000) (generously provided by Baric Lab), mouse anti-streptavidin
607 binding peptide (MAB10764, Millipore, Billerica, MA) (1:10,000), rabbit anti-actin (A2066,
608 Sigma-Aldrich) (1:5,000), and mouse anti-actin (A5441, Sigma-Aldrich) (1:5,000). For
609 quantitative western blotting, the following secondary antibodies from LI-COR were used at a
610 1:20,000 dilution: IRDye 800CW goat anti-mouse (926–32210) and IRDye 680LT goat anti-
611 rabbit (926–68021).

612 ***Generation of mutant ZIKV clones***

613 We used the Baric lab reverse genetics system to generate phosphomimetic and non-
614 phosphorylatable mutants as described in Widman *et al.* (19). ZIKV E was mutated at Y61 to
615 Y61E and Y61F and separately ZIKV E T351 was mutated to T351D and T351A. The Baric
616 reverse genetics system is composed of 4 plasmids, Fragments A through D, that encode the
617 ZIKV proteome. Fragment A was modified by GenScript from thymine to guanine at nucleotide
618 position 1599 and thymine to adenine at position 1601 to generate the Y61E phosphomimetic
619 while nucleotide 1600 was modified from adenine to thymine for the Y61F non-
620 phosphorylatable mutant. Nucleotides 2470 and 2471 in Fragment A were modified from
621 adenine and cytosine to guanine and adenine, respectively, for the T351D phosphomimetic while
622 position 2470 was modified from adenine to guanine for the T351A non-phosphorylatable

623 mutant. Infectious recombinant ZIKV clones were generated as described in Widman *et al.* (19).
624 Four plasmids containing Fragments A-D, respectively, which encode for the ZIKV genome,
625 were digested with BamHI and Bsu36I for Fragment A, Bsu36I and BstXI for Fragment B,
626 BstXI and SfiI for Fragment C, and SfiI, SmaI, AlwNI for Fragment D. Restriction enzymes
627 were all acquired from New England Biolabs (Ipswich, MA). The four digested fragments were
628 ligated with T4 DNA ligase purchased from New England Biolabs. Ligated DNA was
629 precipitated with chloroform then *in vitro* transcribed using the mMESSAGE mMACHINE™ T7
630 ULTRA Transcription Kit from ThermoFisher Scientific. The transcribed product was then
631 electroporated into Vero E6 cells using a Gene Pulser Xcell (Bio-Rad Laboratories, Hercules,
632 CA) and incubated at 37°C for 4 days. Cell media was collected after 4 days and passaged onto a
633 new monolayer of Vero E6 cells. Cell media collected from this passage was described as
634 "passage 1/ p.1". Clarified cell media was titered by plaque assay using Vero E6 cells.

635 ***Virus growth curves***

636 For the Y61F and Y61E mutants, six-well plates were seeded with 2 x 10^5 Vero E6 cells per well
637 and infected the following day at an MOI of 0.001. For the T351A and T351D mutants, 12-well
638 plates were seeded with 2 x 10^4 A549 cells and infected the following day at an MOI of 0.01.
639 Cell media was collected at indicated time points from separate wells. Cell media was clarified
640 by centrifugation at 1200 RPM for 5 minutes, stored at -80°C, and then titered by plaque assay
641 (see plaque and focus assays below for details).

642 ***Plaque and focus assays***

643 Plaque assays were used to measure infectious virus titers in several experiments as follows. Six-
644 well plates were seeded with 2.5 x 10^5 Vero E6 cells per well and the following day inoculated
645 with 10-fold serial dilutions of virus. Plates were rocked every 15 minutes for 1 hour to allow for

646 viral absorption at 37°C, the cells were overlaid with a solution of 0.7% agarose (20–102, Apex
647 Industrial Chemicals, Aberdeen, United Kingdom) in Vero E6 growth media. Wells with agarose
648 plugs were fixed 3 days later with a solution of 2.5% formaldehyde (1635-4L, Sigma-Aldrich) in
649 3x PBS. Following removal of the agarose, the fixed cell monolayers were stained with 0.1%
650 crystal violet (C581-100, Fisher Scientific) and 2.1% ethanol in water.

651 Focus assays were used to assess the presence of the Y61E infectious clones after several
652 viral passages. 24-well plates were seeded with 2 x 10^4 Vero E6 cells per well and the following
653 day were inoculated with 10-fold serial dilutions of infectious viral clones. Plates were incubated
654 for 1 hour at 37°C with rocking every 15 minutes. After absorption, cells were overlaid with
655 0.01% methylcellulose in Vero E6 media (see Cells and Viruses for media detail) and were left
656 in a 37°C incubator for 3 days. After 3 days the overlay was removed and cell monolayers were
657 fixed with 4% formaldehyde (28906, Thermo Fisher Scientific) at room temperature, washed,
658 then permeabalized with 0.5% Triton X-100 in PBS. Cell monolayers were then blocked with
659 5% milk in PBS and thereafter incubated with 4G2 antibody (1:10,000) diluted in 5% milk in
660 PBS for 1 hour at 37°C. Cells were washed with PBS and then incubated with goat anti-mouse
661 secondary antibody at a 1:2000 (5450-0011, LGC Clinical Diagnostics, Inc., Milford, MA)
662 dilution in 5% milk in PBS for 1 hour at 37°C. Cells were washed again and then incubated with
663 TrueBlue Peroxidase Substrate (5510-0030, LGC Clinical Diagnostics, Inc.) until the formation
664 of blue foci and reaction was stopped by removing the substrate.

665 ***Virus-like particle (VLP) release assay***

666 To determine the efficiency of VLP formation and release when ZIKV E contains mutations at
667 Y61 or T351, 5 x 10^5 HEK293T cells in 6-well plates were transfected with 2 µg of the modified
668 PaxVax plasmids (see Plasmids for details) using 8 µg of PEI per well. Twenty-four hours after

669 transfection, fresh cell media was added to wells. 48 hours after transfection, cells and cell media
670 were collected. Cell media was clarified by centrifugation for 3 minutes at 1500 RPM and then
671 VLPs were lysed with 10X Triton buffer for a final dilution of 1X lysis buffer. Cells were
672 collected with cold PBS, centrifuged for 3 minutes at 1500 RPM, and then lysed with Triton
673 buffer. Cells and cell media were subjected to quantitative western blotting for the detection of
674 ZIKV E by way of 4G2 antibody (concentration of 1:10,000). To calculate efficiency of VLP
675 release, each ZIKV E protein value found in cells was first normalized to actin values in cells
676 (rabbit anti-actin antibody at 1:5000). VLP release efficiency was then calculated as the quotient
677 of the E protein quantity in VLPs divided by the quantity of E in cells [(E_{mutant}VLP / E_{mutant}cells)
678 / (E_{WT} VLP/ E_{WT} cells)*100].

679 ***Kinase inhibition assays***

680 To determine if treating cells at the time of infection with various kinase inhibitors would impact
681 viral growth, viral challenge assays were performed. First, to screen a panel of inhibitors at a
682 fixed concentration, 2.5 x 10^5 A549 cells were seeded in 6-well plates. The next day cells were
683 infected at an MOI of 0.1 with ZIKV. After an hour of absorption at 37°C, the inoculum was
684 removed and cells were treated with 10 µM of Sunitinib (B1045, APExBIO Technology LLC,
685 Houston, TX) Bosutinib (PZ0192,Sigma-Aldrich), Defactinib (B4800, APExBIO), Imatinib
686 (9084S, Cell Signaling Technology), or DMSO vehicle control in HEK293T media. The
687 infection proceeded for 48 hours then cell media was collected, clarified by centrifugation, stored
688 at -80°C, and then titered by plaque assay. The percent inhibition was determined by normalizing
689 titers of drug-treated wells to the DMSO control well titers and multiplying by 100. Second, to
690 determine the IC_{50} of Bosutinib or Defactinib, a dose response curve was set up with drugs at
691 concentrations of 30, 20, 15, 10, 7.5, 5, and 1.25 µM as well as DMSO. 2.8 x 10^4 A549 cells

692 were seeded into 48 well plates. One day later, cells were infected at an MOI of 0.1. One hour
693 after absorption, the inoculum was removed and cells were treated with A549 media containing
694 drug at the listed concentrations. After 48 hours, cell media was collected, clarified by
695 centrifugation, stored at -80°C, and then titered by plaque assay. To determine the cell toxicity of
696 each drug, an MTT (3-(4,5-dimethylthiazol-2-yl)-2,5-diphenyltetrazolium bromide)) assay
697 (M6494, Thermo Fisher Scientific) was conducted in parallel to the infection and kinase
698 inhibitor treatment according to manufacturer instructions. A549 cells were set up in 48 well
699 plates and treated with the listed concentrations of Bosutinib. After 48 hours, cell media was
700 removed and replaced with 1.2 mM MTT in PBS for 4 hours at 37°C. After incubation, MTT
701 was removed and DMSO was added to each well, incubated for 10 minutes at 37°C, and
702 absorbance was read at 540 nm. Cell viability was determined by first normalizing the
703 absorbance readings of drug-treated cells to the DMSO control wells. Cell toxicity was
704 determined by subtracting the value of cell viability from 100. To determine the IC_{50} (half-
705 maximal inhibitory concentration) of Bosutinib and Defectinib, we used [inhibitor] versus
706 normalized response curve fitting in Prism 8.0. To determine CC_{50} (cytotoxic concentration
707 causing death to 50% of cells), the same Prism 8.0 curve fitting was applied to our MTT assay
708 data (inhibitor versus cell toxicity). The selectivity index (SI) of each drug was calculated by
709 dividing the CC_{50} by the IC_{50} of each drug.
710

711 **Acknowledgments**

712 We thank the NIH for the following grant support: T32 HL076122 (I.M. and C.M.Z.),
713 R21AI135265 (J.W.B.), P20RR021905 and P30GM118228 (Immunobiology and Infectious
714 Disease COBRE awards) (J.W.B.), AI107731 (R.S.B.), and the National Institute of General

715 Medical Sciences of the NIH (P20GM103449; Vermont Biomedical Research Network
716 Bioinformatics – H.D.; Vermont Biomedical Research Network Proteomics – C.G.). We thank
717 the United Kingdom Research and Innovation Medical Research Council for the following
718 support: ZK/16-012 (D.B) and MR/N008618/1 (E.H.). We also thank the University of Vermont
719 Office of Fellowships, Opportunities and Undergraduate Research for their support of D.T.
720 Funding agencies had no role in study design, collection and analysis of data, manuscript
721 preparation or the decision to publish. We are grateful to Emergent BioSolutions, Inc. and Dr.
722 Lindsay Whitton for kindly providing critical reagents described in the Materials and Methods,
723 Svenja Hester (Advanced Proteomics Facility, University of Oxford) for performing and
724 advising on mass spectrometry, Glasgow Polyomics for computing resources and Dr. Emily
725 Bruce, the UVM Immunobiology group, and the Vermont Lung Center for technical comments
726 and insightful discussions.
727

728 **Conflict of Interests**

729 The authors declare that they have no conflict of interest.

730

731 **References**

732 1. Smithburn KC. Neutralizing antibodies against certain recently isolated viruses in the
733 sera of human beings residing in East Africa. J Immunol. 1952;69(2):223-34. Epub 1952/08/01.
734 PubMed PMID: 14946416.
735 2. Organization PAHOWH. Zika - Epidemiological Report Brazil2017, September 25.
736 3. Cao-Lormeau VM, Blake A, Mons S, Lastere S, Roche C, Vanhomwegen J, Dub T,
737 Baudouin L, Teissier A, Larre P, Vial AL, Decam C, Choumet V, Halstead SK, Willison HJ,

738 Musset L, Manuguerra JC, Despres P, Fournier E, Mallet HP, Musso D, Fontanet A, Neil J,
739 Ghawche F. Guillain-Barre Syndrome outbreak associated with Zika virus infection in French
740 Polynesia: a case-control study. Lancet. 2016;387(10027):1531-9. Epub 2016/03/08. doi:
741 10.1016/S0140-6736(16)00562-6. PubMed PMID: 26948433; PMCID: PMC5444521.
742 4. Mlakar J, Korva M, Tul N, Popovic M, Poljsak-Prijatelj M, Mraz J, Kolenc M, Resman
743 Rus K, Vesnaver Vipotnik T, Fabjan Vodusek V, Vizjak A, Pizem J, Petrovec M, Avsic Zupanc
744 T. Zika Virus Associated with Microcephaly. N Engl J Med. 2016;374(10):951-8. doi:
745 10.1056/NEJMoa1600651. PubMed PMID: 26862926.
746 5. Hemonnot B, Cartier C, Gay B, Rebuffat S, Bardy M, Devaux C, Boyer V, Briant L. The
747 host cell MAP kinase ERK-2 regulates viral assembly and release by phosphorylating the p6gag
748 protein of HIV-1. J Biol Chem. 2004;279(31):32426-34. Epub 2004/05/25. doi:
749 10.1074/jbc.M313137200. PubMed PMID: 15155723.
750 6. Ziegler CM, Eisenhauer P, Bruce EA, Weir ME, King BR, Klaus JP, Krementsov DN,
751 Shirley DJ, Ballif BA, Botten J. The Lymphocytic Choriomeningitis Virus Matrix Protein PPXY
752 Late Domain Drives the Production of Defective Interfering Particles. PLoS pathogens.
753 2016;12(3):e1005501. doi: 10.1371/journal.ppat.1005501. PubMed PMID: 27010636; PMCID:
754 PMC4806877.
755 7. Ziegler CM, Eisenhauer P, Bruce EA, Beganovic V, King BR, Weir ME, Ballif BA,
756 Botten J. A novel phosphoserine motif in the LCMV matrix protein Z regulates the release of
757 infectious virus and defective interfering particles. J Gen Virol. 2016. doi: 10.1099/jgv.0.000550.
758 PubMed PMID: 27421645.
759 8. Ziegler CM, Eisenhauer P, Manuelyan I, Weir ME, Bruce EA, Ballif BA, Botten J. Host-
760 Driven Phosphorylation Appears to Regulate the Budding Activity of the Lassa Virus Matrix

761 Protein. Pathogens. 2018;7(4). doi: 10.3390/pathogens7040097. PubMed PMID: 30544850;
762 PMCID: PMC6313517.
763 9. Bhattacharya D, Hoover S, Falk SP, Weisblum B, Vestling M, Striker R. Phosphorylation
764 of yellow fever virus NS5 alters methyltransferase activity. Virology. 2008;380(2):276-84. doi:
765 10.1016/j.virol.2008.07.013. PubMed PMID: 18757072; PMCID: PMC2583469.
766 10. Kapoor M, Zhang L, Ramachandra M, Kusukawa J, Ebner KE, Padmanabhan R.
767 Association between NS3 and NS5 proteins of dengue virus type 2 in the putative RNA replicase
768 is linked to differential phosphorylation of NS5. J Biol Chem. 1995;270(32):19100-6. PubMed
769 PMID: 7642575.
770 11. Yamauchi S, Takeuchi K, Chihara K, Sun X, Honjoh C, Yoshiki H, Hotta H, Sada K.
771 Hepatitis C Virus Particle Assembly Involves Phosphorylation of NS5A by the c-Abl Tyrosine
772 Kinase. J Biol Chem. 2015;290(36):21857-64. Epub 2015/07/24. doi: 10.1074/jbc.M115.666859.
773 PubMed PMID: 26203192; PMCID: PMC4571941.
774 12. Quintavalle M, Sambucini S, Summa V, Orsatti L, Talamo F, De Francesco R,
775 Neddermann P. Hepatitis C virus NS5A is a direct substrate of casein kinase I-alpha, a cellular
776 kinase identified by inhibitor affinity chromatography using specific NS5A
777 hyperphosphorylation inhibitors. J Biol Chem. 2007;282(8):5536-44. Epub 2006/12/15. doi:
778 10.1074/jbc.M610486200. PubMed PMID: 17166835.
779 13. Tellinghuisen TL, Foss KL, Treadaway J. Regulation of hepatitis C virion production via
780 phosphorylation of the NS5A protein. PLoS pathogens. 2008;4(3):e1000032. doi:
781 10.1371/journal.ppat.1000032. PubMed PMID: 18369478; PMCID: PMC2265800.
782 14. Henchal EA, Gentry MK, McCown JM, Brandt WE. Dengue virus-specific and flavivirus
783 group determinants identified with monoclonal antibodies by indirect immunofluorescence. Am

784 J Trop Med Hyg. 1982;31(4):830-6. Epub 1982/07/01. doi: 10.4269/ajtmh.1982.31.830. PubMed
785 PMID: 6285749.
786 15. King BR, Hershkowitz D, Eisenhauer PL, Weir ME, Ziegler CM, Russo J, Bruce EA,
787 Ballif BA, Botten J. A map of the arenavirus nucleoprotein-host protein interactome reveals that
788 Junin virus selectively impairs the antiviral activity of PKR. J Virol. 2017. doi:
789 10.1128/JVI.00763-17. PubMed PMID: 28539447.
790 16. Mukhopadhyay S, Kuhn RJ, Rossmann MG. A structural perspective of the flavivirus life
791 cycle. Nat Rev Microbiol. 2005;3(1):13-22. Epub 2004/12/21. doi: 10.1038/nrmicro1067.
792 PubMed PMID: 15608696.
793 17. Akey DL, Brown WC, Dutta S, Konwerski J, Jose J, Jurkiw TJ, DelProposto J, Ogata
794 CM, Skiniotis G, Kuhn RJ, Smith JL. Flavivirus NS1 structures reveal surfaces for associations
795 with membranes and the immune system. Science. 2014;343(6173):881-5. Epub 2014/02/08. doi:
796 10.1126/science.1247749. PubMed PMID: 24505133; PMCID: PMC4263348.
797 18. Rastogi M, Sharma N, Singh SK. Flavivirus NS1: a multifaceted enigmatic viral protein.
798 Virol J. 2016;13:131. Epub 2016/07/31. doi: 10.1186/s12985-016-0590-7. PubMed PMID:
799 27473856; PMCID: PMC4966872.
800 19. Widman DG, Young E, Yount BL, Plante KS, Gallichotte EN, Carbaugh DL, Peck KM,
801 Plante J, Swanstrom J, Heise MT, Lazear HM, Baric RS. A Reverse Genetics Platform That
802 Spans the Zika Virus Family Tree. MBio. 2017;8(2). doi: 10.1128/mBio.02014-16. PubMed
803 PMID: 28270583; PMCID: PMC5340872.
804 20. Espinosa D, Mendy J, Manayani D, Vang L, Wang C, Richard T, Guenther B, Aruri J,
805 Avanzini J, Garduno F, Farness P, Gurwith M, Smith J, Harris E, Alexander J. Passive Transfer
806 of Immune Sera Induced by a Zika Virus-Like Particle Vaccine Protects AG129 Mice Against

807 Lethal Zika Virus Challenge. EBioMedicine. 2018;27:61-70. Epub 2017/12/23. doi:
808 10.1016/j.ebiom.2017.12.010. PubMed PMID: 29269041; PMCID: PMC5828544.
809 21. Tabata K, Arimoto M, Arakawa M, Nara A, Saito K, Omori H, Arai A, Ishikawa T,
810 Konishi E, Suzuki R, Matsuura Y, Morita E. Unique Requirement for ESCRT Factors in
811 Flavivirus Particle Formation on the Endoplasmic Reticulum. Cell Rep. 2016;16(9):2339-47.
812 Epub 2016/08/23. doi: 10.1016/j.celrep.2016.07.068. PubMed PMID: 27545892.
813 22. Giraldo MI, Xia H, Aguilera-Aguirre L, Hage A, van Tol S, Shan C, Xie X, Sturdevant
814 GL, Robertson SJ, McNally KL, Meade-White K, Azar SR, Rossi SL, Maury W, Woodson M,
815 Ramage H, Johnson JR, Krogan NJ, Morais MC, Best SM, Shi PY, Rajsbaum R. Envelope
816 protein ubiquitination drives entry and pathogenesis of Zika virus. Nature. 2020;585(7825):414-
817 9. Epub 2020/07/10. doi: 10.1038/s41586-020-2457-8. PubMed PMID: 32641828; PMCID:
818 PMC7501154.
819 23. Ziegler CM, Dang L, Eisenhauer P, Kelly JA, King BR, Klaus JP, Manuelyan I, Mattice
820 EB, Shirley DJ, Weir ME, Bruce EA, Ballif BA, Botten J. NEDD4 family ubiquitin ligases
821 associate with LCMV Z's PPXY domain and are required for virus budding, but not via direct
822 ubiquitination of Z. PLoS pathogens. 2019;15(11):e1008100. Epub 2019/11/12. doi:
823 10.1371/journal.ppat.1008100. PubMed PMID: 31710650; PMCID: PMC6874086
824 24. Pierson TC, Diamond MS. Degrees of maturity: the complex structure and biology of
825 flaviviruses. Curr Opin Virol. 2012;2(2):168-75. Epub 2012/03/27. doi:
826 10.1016/j.coviro.2012.02.011. PubMed PMID: 22445964; PMCID: PMC3715965.
827 25. Bhattacharya D, Mayuri, Best SM, Perera R, Kuhn RJ, Striker R. Protein kinase G
828 phosphorylates mosquito-borne flavivirus NS5. J Virol. 2009;83(18):9195-205. doi:
829 10.1128/JVI.00271-09. PubMed PMID: 19587048; PMCID: PMC2738234.

830 26. Morozova OV, Tsekhanovskaya NA, Maksimova TG, Bachvalova VN, Matveeva VA,
831 Kit Y. Phosphorylation of tick-borne encephalitis virus NS5 protein. Virus Res. 1997;49(1):9-15.
832 PubMed PMID: 9178492.
833 27. Lemay KL, Treadaway J, Angulo I, Tellinghuisen TL. A hepatitis C virus NS5A
834 phosphorylation site that regulates RNA replication. J Virol. 2013;87(2):1255-60. Epub
835 2012/11/02. doi: 10.1128/JVI.02154-12. PubMed PMID: 23115292; PMCID: PMC3554050.
836 28. Valencia HJ, de Aguiar M, Costa MA, Mendonca DC, Reis EV, Arias NEC, Drumond
837 BP, Bonjardim CA. Evaluation of kinase inhibitors as potential therapeutics for flavivirus
838 infections. Arch Virol. 2021;166(5):1433-8. Epub 2021/03/09. doi: 10.1007/s00705-021-05021-
839 1. PubMed PMID: 33683474; PMCID: PMC7938686.
840 29. Lee CY, Henricks DM, Skelley GC, Grimes LW. Growth and hormonal response of
841 intact and castrate male cattle to trenbolone acetate and estradiol. J Anim Sci. 1990;68(9):2682-
842 9. Epub 1990/09/01. doi: 10.2527/1990.6892682x. PubMed PMID: 2211398.
843 30. Rausch K, Hackett BA, Weinbren NL, Reeder SM, Sadovsky Y, Hunter CA, Schultz DC,
844 Coyne CB, Cherry S. Screening Bioactives Reveals Nanchangmycin as a Broad Spectrum
845 Antiviral Active against Zika Virus. Cell Rep. 2017;18(3):804-15. Epub 2017/01/19. doi:
846 10.1016/j.celrep.2016.12.068. PubMed PMID: 28099856; PMCID: PMC5270376.
847 31. Liang Q, Luo Z, Zeng J, Chen W, Foo SS, Lee SA, Ge J, Wang S, Goldman SA,
848 Zlokovic BV, Zhao Z, Jung JU. Zika Virus NS4A and NS4B Proteins Deregulate Akt-mTOR
849 Signaling in Human Fetal Neural Stem Cells to Inhibit Neurogenesis and Induce Autophagy.
850 Cell Stem Cell. 2016;19(5):663-71. doi: 10.1016/j.stem.2016.07.019. PubMed PMID: 27524440;
851 PMCID: PMC5144538.

852 32. Chiramel AI, Best SM. Role of autophagy in Zika virus infection and pathogenesis. Virus
853 Res. 2018;254:34-40. Epub 2017/09/14. doi: 10.1016/j.virusres.2017.09.006. PubMed PMID:
854 28899653; PMCID: PMC5844781.
855 33. Scaturro P, Stukalov A, Haas DA, Cortese M, Draganova K, Plaszczyca A,
856 Bartenschlager R, Gotz M, Pichlmair A. An orthogonal proteomic survey uncovers novel Zika
857 virus host factors. Nature. 2018;561(7722):253-7. Epub 2018/09/05. doi: 10.1038/s41586-018-
858 0484-5. PubMed PMID: 30177828.
859 34. Donald CL, Brennan B, Cumberworth SL, Rezelj VV, Clark JJ, Cordeiro MT, Freitas de
860 Oliveira Franca R, Pena LJ, Wilkie GS, Da Silva Filipe A, Davis C, Hughes J, Varjak M,
861 Selinger M, Zuvanov L, Owsianka AM, Patel AH, McLauchlan J, Lindenbach BD, Fall G, Sall
862 AA, Biek R, Rehwinkel J, Schnettler E, Kohl A. Full Genome Sequence and sfRNA Interferon
863 Antagonist Activity of Zika Virus from Recife, Brazil. PLoS Negl Trop Dis.
864 2016;10(10):e0005048. Epub 2016/10/06. doi: 10.1371/journal.pntd.0005048. PubMed PMID:
865 27706161; PMCID: PMC5051680.
866 35. Alzhanova D, Corcoran K, Bailey AG, Long K, Taft-Benz S, Graham RL, Broussard GS,
867 Heise M, Neumann G, Halfmann P, Kawaoka Y, Baric RS, Damania B, Dittmer DP. Novel
868 modulators of p53-signaling encoded by unknown genes of emerging viruses. PLoS pathogens.
869 2021;17(1):e1009033. Epub 2021/01/08. doi: 10.1371/journal.ppat.1009033. PubMed PMID:
870 33411764; PMCID: PMC7790267
871 36. Klaus JP, Eisenhauer P, Russo J, Mason AB, Do D, King B, Taatjes D, Cornillez-Ty C,
872 Boyson JE, Thali M, Zheng C, Liao L, Yates JR, 3rd, Zhang B, Ballif BA, Botten JW. The
873 intracellular cargo receptor ERGIC-53 is required for the production of infectious arenavirus,

874 coronavirus, and filovirus particles. Cell Host Microbe. 2013;14(5):522-34. Epub 2013/11/19.
875 doi: 10.1016/j.chom.2013.10.010. PubMed PMID: 24237698; PMCID: 3999090.
876 37. Cornillez-Ty CT, Liao L, Yates JR, 3rd, Kuhn P, Buchmeier MJ. Severe acute respiratory
877 syndrome coronavirus nonstructural protein 2 interacts with a host protein complex involved in
878 mitochondrial biogenesis and intracellular signaling. J Virol. 2009;83(19):10314-8. Epub
879 2009/07/31. doi: JVI.00842-09 [pii] 10.1128/JVI.00842-09. PubMed PMID: 19640993; PMCID:
880 2748024.
881 38. Hutchinson EC, Stegmann M. Purification and Proteomics of Influenza Virions. Methods
882 Mol Biol. 2018;1836:89-120. Epub 2018/08/29. doi: 10.1007/978-1-4939-8678-1_5. PubMed
883 PMID: 30151570.
884 39. Wisniewski JR, Zougman A, Nagaraj N, Mann M. Universal sample preparation method
885 for proteome analysis. Nat Methods. 2009;6(5):359-62. Epub 2009/04/21. doi:
886 10.1038/nmeth.1322. PubMed PMID: 19377485.
887 40. Tyanova S, Temu T, Cox J. The MaxQuant computational platform for mass
888 spectrometry-based shotgun proteomics. Nat Protoc. 2016;11(12):2301-19. Epub 2016/11/04.
889 doi: 10.1038/nprot.2016.136. PubMed PMID: 27809316.
890 41. Edgar RC. MUSCLE: multiple sequence alignment with high accuracy and high
891 throughput. Nucleic Acids Res. 2004;32(5):1792-7. Epub 2004/03/23. doi: 10.1093/nar/gkh340.
892 PubMed PMID: 15034147; PMCID: PMC390337.
893 42. Pickett BE, Sadat EL, Zhang Y, Noronha JM, Squires RB, Hunt V, Liu M, Kumar S,
894 Zaremba S, Gu Z, Zhou L, Larson CN, Dietrich J, Klem EB, Scheuermann RH. ViPR: an open
895 bioinformatics database and analysis resource for virology research. Nucleic Acids Res.

896 2012;40(Database issue):D593-8. Epub 2011/10/19. doi: 10.1093/nar/gkr859. PubMed PMID:
897 22006842; PMCID: PMC3245011.
898 43. Waterhouse AM, Procter JB, Martin DM, Clamp M, Barton GJ. Jalview Version 2--a
899 multiple sequence alignment editor and analysis workbench. Bioinformatics. 2009;25(9):1189-
900 91. Epub 2009/01/20. doi: 10.1093/bioinformatics/btp033. PubMed PMID: 19151095; PMCID:
901 PMC2672624.

902 **Figure Legends**

903 **Figure 1. Discovery of post-translational modifications on the ZIKV proteome.**

904 (A) Depictions of i) a ZIKV particle with its structural proteins indicated and ii) the organization
905 of the ZIKV positive-strand RNA genome and its encoded ORFeome.

906 (B) Overview of the workflow for discovery of post-translational modifications on ZIKV
907 proteins in the settings of viral infection or plasmid-based expression of ZIKV proteins. IP,
908 immunoprecipitation; AP, affinity purification.

909 (C, D, and E) Western blots and Coomassie stained SDS-page gels of affinity purified ZIKV E
910 from ZIKV infected cells (C), authentic ZIKV particles (D), or the indicated SBP-tagged ZIKV
911 proteins (E). For (C and D), Vero E6 cells were infected with ZIKV strain BeH819015 at an
912 MOI of 0.1. Cells (C) and media (D) were collected 72 hours and 96 hours later, respectively. In
913 (C), infected cells were lysed in Triton-X buffer and intracellular ZIKV E was purified using the
914 anti-E antibody 4G2 and magnetic protein G beads. As a control, we performed
915 immunoprecipitation of uninfected (mock) cellular lysates with the 4G2 antibody. In (D), viral
916 particles were immunoprecipitated from clarified supernatants using the 4G2 antibody and
917 magnetic protein G beads. Control conditions included (i) immunoprecipitation of virus-
918 containing supernatants with a non-specific mouse IgG antibody and (ii) immunoprecipitation of
919 an uninfected (mock) supernatant with the 4G2 antibody. For (E), to purify ZIKV proteins
920 expressed from plasmid, we engineered plasmids to encode the indicated ZIKV ORFs with a C-
921 terminal streptavidin-binding protein (SBP) tag. HEK293T cells were transfected with a plasmid
922 encoding the indicated SBP-tagged ZIKV protein or, as a control, an empty vector (V). Two days
923 after transfection, the cells were lysed in Triton-X buffer and ZIKV proteins were affinity
924 purified using streptavidin-coated magnetic beads (labeled as Anti-SBP in panels). In panels (C-

925 E), for both antibody- and streptavidin-based purifications, captured protein mixtures were
926 orthogonally separated using SDS-PAGE, followed by in-gel processing for subsequent mass
927 spectrometry analysis to discover post-translational modifications or interacting host proteins.
928 The molecular weight in kDa, viral proteins (yellow text and arrows), and immunoglobulin
929 bands are labeled. Note that the asterisks in (E) indicate monomeric streptavidin that was eluted
930 off the streptavidin beads when boiled.
931
932 **Figure 2. Location of post-translational modification sites on ZIKV proteins.** Phosphosites
933 and ubiquitination sites are marked in green and light purple, respectively. For each ZIKV
934 protein, individual domains or specific features are color coded with the text label displayed in
935 the matching color in each instance.
936 (A and B) Location of the Y61 and T351 phosphosites on ZIKV E (A) or location of all post-
937 translational modifications on ZIKV E (B). In both (A and B), PDB ID: 5JHM was used and one
938 copy of E is shown.
939 (C) ZIKV E - M heterodimer (PDB ID: 5IZ7). Y61 and T351 are labeled on the E ectodomain.
940 ZIKV M phosphosites S16 and T18 are labeled on the M protein.
941 (D) PTM locations on ZIKV NS1 (PDB ID: 5GS6).
942 (E) ZIKV NS2B – NS3 protease complex shown in close conformation (PDB ID: 5GPI) with
943 labeled phosphosites on ZIKV NS2B.
944 (F) ZIKV NS5 (PDB ID: 5TMH) phosphosites. RdRp, RNA-dependent RNA polymerase;
945 MTase, methyltransferase domain.
946

947 **Figure 3. Tyrosine 61 and threonine 351 on the ZIKV E protein are critical for viral**
948 **propagation at the stage of viral budding.**
949 (A-C) Overview of the reverse genetics approach used to recover infectious ZIKV clones bearing
950 mutations at Y61 or T351 in the E protein (A). For each recovery attempt, full-length infectious
951 RNAs were transcribed from a cDNA template of the viral genome. The RNAs were
952 electroporated into Vero E6 cells and 3 days later supernatants from these cultures were screened
953 for the presence of infectious ZIKV particles by either viral plaque assay (B) or focus assay (C).
954 In (C), the rZIKV E Y61E clone was passaged 2 additional times due to the absence of
955 detectable plaques or foci after passage 1. The Y61E passage 3 material showed infectious virus
956 and this rLCMV had mutated from a glutamic acid to a valine at position 61.
957 (D and E) The growth kinetics of the indicated rZIKV E Y61 mutants (D) or T351 mutants (E)
958 was determined by infecting Vero E6 cells at an MOI of 0.001 (D) or A549 cells at an MOI of
959 0.01 (E) with these viruses and measuring the infectious particles released by plaque assay at 24,
960 48, 72, 96, 120, or 144 hours after infection. Data represent the mean±SEM from three (D) or
961 two (E) independent biological replicates. For statistical analysis, data were analyzed via mixed-
962 effect analysis (two-way ANOVA) with Holm-Sidak's test for multiple comparisons in Prism
963 8.0.
964 (F) The budding activity of WT, Y61- or T351-mutant E proteins was measured by a virus-like
965 particle (VLP) assay. VLPs were generated by transfection of HEK293T cells with plasmid that
966 encodes ZIKV prM and E (either WT E or the indicated E mutants). The quantity of ZIKV E
967 released into the supernatant vs retained in cells was measured by quantitative western blot and
968 budding efficiency was determined as described in the Methods. Data represent the mean±SEM

969 from three (Y61 mutants) or four (T351 mutants) independent biological replicates. Statistical
970 significance was determined in Prism 8.0 software using a one-way ANOVA.
971 For the indicated statistical tests in (D-F): *, P<0.05; **; P<0.01; ***; P<0.001.
972
973 **Figure 4. Host kinase interactions the ZIKV proteome and effects of kinase inhibitors on**
974 **ZIKV growth.**
975 **(**A) Host kinases that interact with ZIKV proteins. Shown are kinases that had the greatest
976 number of tryptic peptides (top 10 for each ZIKV protein) detected by mass spectrometry and/or
977 were predicted by Scansite 4.0 to phosphorylate one or more of the phosphosites identified in
978 this study. Black circles denote kinases that interacted with 5 viral proteins. ZIKV proteins with
979 detectable phosphosites in this study are indicated with a "P". Drugs known to inhibit specific
980 kinases are listed; drugs with FDA approval are bolded.
981 (B) Efficacy of kinase inhibitors in restricting ZIKV growth. A549 cells were infected with
982 ZIKV at a MOI of 0.1 and 1 hour later, the inoculum was removed and cells were treated with 10
983 μM of the indicated drug or, as a control, DMSO (vehicle). Two days later infectious virus
984 measured in the supernatants via plaque assay. Data represent mean±SEM from three
985 independent biological replicates. Statistical significance was determined in Prism 8.0 software
986 via one-way ANOVA with Holm-Sidak's test for multiple comparisons. *, P<0.05
987 (C and D) IC_{50} determination for Defactinib and Bosutinib inhibition of ZIKV growth. A549
988 cells were infected with ZIKV at a MOI of 0.1 and 1 hour later, the inoculum was removed and
989 cells were treated with the indicated doses of Bosutinib or Defactinib. Two days later infectious
990 virus was measured in the supernatants via plaque assay. In parallel, the cytotoxicity of each
991 drug at these same doses was determined via MTT assay as described in the Methods. Data

992 represent mean±SEM from three independent biological replicates. The resulting IC_{50} and
993 selective index (SI) values are listed for each drug. Calculations of both values are described in
994 Methods.
995
996 **Figure S1. Identification of ZIKV E phosphosite T351 in virions from mosquito cells.** C6/36
997 mosquito cells were inoculated with ZIKV at an MOI of 0.1. Four days later, cell-free ZIKV
998 particles were collected, concentrated, and purified by banding on a potassium tartrate density
999 gradient. (A) Aliquots of gradient fractions were separated by SDS-PAGE and stained with
1000 Coomassie Brilliant Blue; the position of ZIKV E is shown. Virus-containing fractions then were
1001 dialyzed and concentrated. (B) Negative stain transmission electron micrograph showing
1002 concentrated ZIKV virions prepared using this process (from an infection at MOI of 1.0,
1003 harvested at 72 h post-infection). Concentrated ZIKV particles were digested with trypsin and
1004 LysC and analyzed using mass spectrometry. Annotated mass spectra are shown for ZIKV E
1005 T351 in (C) unmodified site and (D) phosphorylated forms*;* ph/@ = phosphorylation.
1006
1007 **Figure S2. Purification of plasmid-expressed ZIKV M, C, or E in the setting of phosphatase**
1008 **inhibition for mass spectrometry analysis.** Western blots and Coomassie stained SDS-page
1009 gels of purified SBP-tagged ZIKV proteins. HEK293T cells were transfected with a plasmid
1010 encoding the indicated SBP-tagged ZIKV protein or, as a control, an empty vector (V). Two days
1011 after transfection, cells were treated with DMSO, H_2O_2, or Calyculin A for 30 minutes and then
1012 lysed in Triton-X buffer. SBP-tagged ZIKV proteins were affinity purified using streptavidin-
1013 coated magnetic beads and the captured protein mixtures were orthogonally separated using
1014 SDS-PAGE, followed by in-gel processing for subsequent mass spectrometry analysis to

1015 discover post-translational modifications or interacting host proteins. The molecular weight in
1016 kDa, viral proteins (yellow text and arrows), and immunoglobulin bands are labeled. Note that
1017 the asterisks in indicate monomeric streptavidin that was eluted off of the streptavidin beads
1018 when boiled.
1019
1020 **Figure S3 Purification of plasmid-expressed ZIKV NS1, NS4A, and NS2B in the setting of**
1021 **phosphatase inhibition for mass spectrometry analysis.** Western blots and Coomassie stained
1022 SDS-page gels of purified SBP-tagged ZIKV proteins. HEK293T cells were transfected with a
1023 plasmid encoding the indicated SBP-tagged ZIKV protein or, as a control, an empty vector (V).
1024 Two days after transfection, cells were treated with DMSO, H_2O_2, or Calyculin A for 30 minutes
1025 and then lysed in Triton-X buffer. SBP-tagged ZIKV proteins were affinity purified using
1026 streptavidin-coated magnetic beads and the captured protein mixtures were orthogonally
1027 separated using SDS-PAGE, followed by in-gel processing for subsequent mass spectrometry
1028 analysis to discover post-translational modifications or interacting host proteins. The molecular
1029 weight in kDa, viral proteins (yellow text and arrows), and immunoglobulin bands are labeled.
1030 Note that the asterisks in indicate monomeric streptavidin that was eluted off streptavidin beads
1031 when boiled.
1032
1033 **Figure S4. Purification of plasmid expressed ZIKV NS4B and NS5 in the setting of**
1034 **phosphatase inhibition for mass spectrometry analysis.** Western blots and Coomassie stained
1035 SDS-page gels of purified SBP-tagged ZIKV proteins. HEK293T cells were transfected with a
1036 plasmid encoding the indicated SBP-tagged ZIKV protein or, as a control, an empty vector (V).
1037 Two days after transfection, cells were treated with DMSO, H_2O_2, or Calyculin A for 30 minutes

1038 and then lysed in Triton-X buffer. SBP-tagged ZIKV proteins were affinity purified using
1039 streptavidin-coated magnetic beads and the captured protein mixtures were orthogonally
1040 separated using SDS-PAGE, followed by in-gel processing for subsequent mass spectrometry
1041 analysis to discover post-translational modifications or interacting host proteins. The molecular
1042 weight in kDa, viral proteins (yellow text and arrows), and immunoglobulin bands are labeled.
1043 Note that the asterisks in indicate monomeric streptavidin that was eluted off of the streptavidin
1044 beads when boiled.
1045
1046 **Figure S5. PTMs labeled on an electrostatic model of ZIKV E dimer** (PDB ID: 5JHM). Blue
1047 indicates positive charges while red indicates negative charges. (A) Electrostatic view of ZIKV E
1048 dimer. (B) rotated to the negatively charged "face". (C) "Side-view" positioning showing the
1049 neutral border of electrostatically labeled ZIKV E dimer along with location of post-translational
1050 modification.
1051
1052 **Figure S6. ZIKV E Y61 interactions with neighboring residues and a view of the junction**
1053 **of ZIKV E and M.** (A) Zoomed in view of the junction of ZIKV E (yellow) and M heterodimer
1054 (dark purple) with M phosphosites labeled in green. (B) Zoomed in view of Y61 on ZIKV E.
1055 Y61 is labeled in green while residues in close proximity, N207 and E262, are labeled in yellow.
1056
1057 **Figure S7. NS2A and NS3 did not express at sufficiently high levels for mass spectrometry**
1058 **analysis.** Attempts were made to express and purify NS2A and NS3 via plasmid transfection of
1059 mammalian cells. HEK293T cells were transfected with plasmids that encoded ZIKV proteins
1060 with either a C-terminal 3x FLAG-tag (A) or a SBP tag (B). Two days later, cells were lysed and

1061 tag-based protein purifications were attempted with an anti-FLAG antibody and magnetic protein

1062 G beads (A) or magnetic streptavidin beads (B).

1063

1064

1065 **Table 1. Phosphorylation and ubiquitination sites on the ZIKV proteome.**

ZIKV Protein	Post-translational modifications	Treatment[a]			Predicted Kinases/Interacting kinases/ Closely-related kinases discovered[b]
		DMSO	H_2O_2	Calyculin A	
C	None found				
M	S16‡[c]			✓	PRKAA1, NEK1, NEK3, NEK4, NEK5, NEK8, NEK10 (low), CLK2, ATM, PRKDC (min)
	T18			✓	GSK3B, AKT1, PRKACG (low), CAMK2B, PRKCE, PRKAA1, AURKA, AURKB (min)
E	Y61^[d]				FGR
	S142	✓	✓	✓	GSK3B, AURKB, NEK3 (min)
	S149	✓	✓	✓	PRKAA1, NEK5 (min)
	T156	✓			GSK3B, PLK1, PRKAA1 (min)
	S173^	✓	✓	✓	CDK1, CDK5 (low), MAPK3 (min)
	T179		✓	✓	PLK1, PRKCD, PRKCE, PRKAA1, AURKA, NEK6, NEK7, NEK10 (min)
	S185‡	✓		✓	
	T205			✓	NEK7 (med), NEK6, NEK8, NEK9 (low), NEK 10 (min)
	T231	✓	✓	✓	NEK6, MAPK3 (min)
	T233		✓	✓	CDK1, CDK5 (low) MAPK3 (low)
	T254			✓	PRKACG, AURKB (med), PRKCD, PRKAA1, AURKA (low), CAMK2G, PRKCE, PRKD1, NEK2, NEK4, NEK5 (min)
	S306^			✓	PLK1, AKT1, AURKA (min)
	T335	✓	✓	✓	CSNK1G2 (min)
	T351‡	✓	✓	✓	CAMK2G (min)
	T353	✓	✓	✓	CDK1, CDK5, MAPK3 (low)
	T360^^[e]			✓	AKT1 (low), PRKD1, MAPK3 (min)
	T366			✓	
	S368			✓	
	S372			✓	NEK5 (low), CSNK1G2, PLK1 (min)
	K93^	✓	✓	✓	
	K118^		✓		
	K246	✓			
	K281^	✓	✓		
	K290	✓	✓		
NS1	T17‡*[f]	✓			PRKD1, PRKCZ (low) AKT1, PRKACG, PRKCA, PRKCD (min)
	Y22*	✓			FGR, LCK, SCR (min)
	S132	✓	✓	✓	PLK1 (med), NEK5 (low), CAMK2G, PRKCD, PDPK1, NEK1, NEK5, NEK9, NEK10 (min)
	Y175		✓		INSR (min)
	S176	✓		✓	PLK1 (low)

	T186			✓	CDK1 (min)
	Y200		✓		NEK10 (min)
	T233**[g]		✓		CSNK1G2 (min)
	S239**^^		✓		
	S246^			✓	PRKD1 (min)
	S348^^	✓	✓	✓	NEK2 (med), NEK1, NEK3, NEK4, NEK8, NEK10 (low), NEK5, NEK6, NEK9 (min)
	K141		✓		
NS2B	S71^		✓	✓	CDK1, CDK5 (low)
NS4A	None found				
NS2A	No expression				
NS3	No expression				
NS4B	S217#[h]/S218#‡/ T219#		✓		PRKAA1 (low), NEK6, NEK8, NEK9, GSK3B, PLK1, PDPK1, CDK1 (min)
NS5	S234			✓	CDK1 (min)
	S237^^			✓	PRKAA1, PRKDC, NEK3, NEK10 (min)
	T292^	✓			PRKCD, PRKCE, NEK6, NEK7, NEK8 (min)
	S663^^	✓	✓	✓	CLK2 (min)

[a]Cell treatment conditions (DMSO, H_2O_2, Calyculin A, or, in the case of Y61, no treatment) under peptides were detected are indicated with check marks.

[b]Names in black text represent kinases predicted by Scansite 4.0 to phosphorylate the corresponding residue listed in a given row. Purple text represents predicted kinases that were also interacting partners of the indicated viral protein for a particular row. Blue text represents predicted kinases that were not found to interact with viral proteins but are in the same kinase cascade or has shared homology with an interacting kinase. Predicted kinases are followed by Scansite 4.0 stringency levels (high, med/medium, low, or min/minimum). High, medium, low, minimum stringency indicates that the motif identified in the ZIKV polypeptide sequence is within the top 0.2%, 1%, 5% and 15% of sequence matches, respectively.

[c]‡Phosphosite conserved only among ZIKV strains.

[d]^Phosphosite conserved in 7 or more of the 15 *Flavivirus* genus members analyzed.

[e]^^ Phosphosite highly conserved among 13 or more *Flavivirus* genus members analyzed.

1079 -For full details of the amino acid conservation analysis related to [c,d,e], see the "multiple sequence

1080 alignment" section of the Methods.

1081 [f*]Mass spectrometry data not sufficient to distinguish between NS1 sites T17 and Y22; there was

1082 evidence for both sites.

1083 [g**]Evidence for both NS1 T233 and S239 sites.

1084 [h#]Phosphosite was located to one of these three locations.

Figure 1

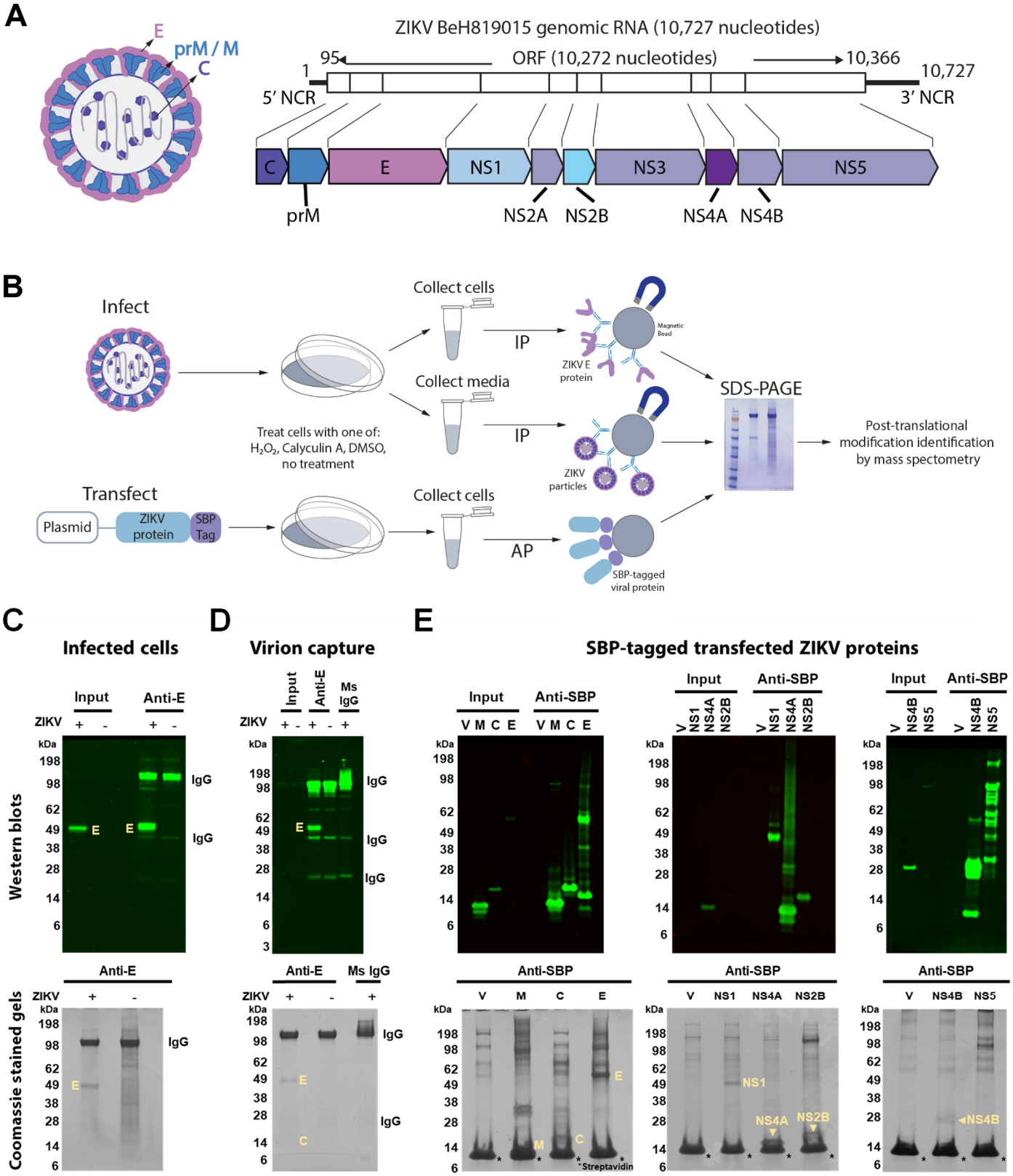
A
E
prM / M
C
ZIKV BeH819015 genomic RNA (10,727 nucleotides)
95
ORF (10,272 nucleotides)
10,366
1
10,727
5′ NCR
3′ NCR
C
E
NS1
NS3
NS5
prM
NS2A
NS2B
NS4A
NS4B
B
Infect
Collect cells
IP
Magnetic Bead
ZIKV E protein
Collect media
IP
ZIKV particles
SDS-PAGE
Post-translational modification identification by mass spectometry
Treat cells with one of: H2O2, Calyculin A, DMSO, no treatment
Transfect
Plasmid
ZIKV protein
SBP Tag
Collect cells
AP
SBP-tagged viral protein
C
Infected cells
Input
Anti-E
ZIKV
kDa
198
98
62
49
38
28
14
6
E
IgG
Western blots
Coomassie stained gels
D
Virion capture
Input
Anti-E
Ms IgG
3
C
E
SBP-tagged transfected ZIKV proteins
Input
Anti-SBP
V M C E
V NS1 NS4A NS2B
V NS4B NS5
M
NS1
NS4A
NS2B
NS4B
NS5
*Streptavidin

Figure 2

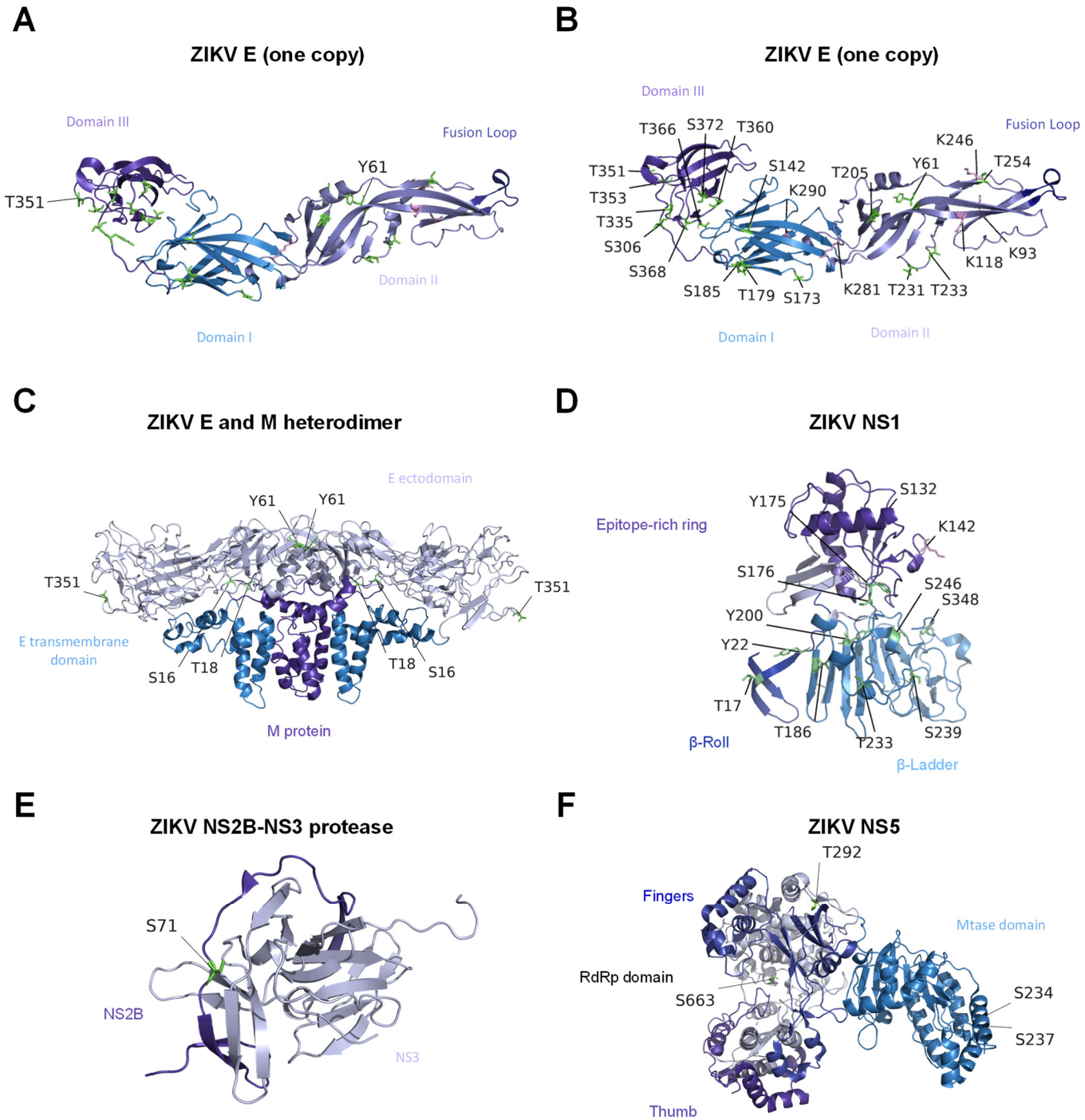
A
ZIKV E (one copy)
Domain III
Fusion Loop
Y61
T351
Domain II
Domain I
B
ZIKV E (one copy)
Domain III
T366
S372
T360
Fusion Loop
K246
T351
S142
T205
Y61
T254
T353
K290
T335
S306
K118
K93
S368
S185
T179
S173
K281
T231
T233
Domain I
Domain II
C
ZIKV E and M heterodimer
E ectodomain
Y61
Y61
T351
T351
E transmembrane domain
S16
T18
T18
S16
M protein
D
ZIKV NS1
S132
Y175
Epitope-rich ring
K142
S176
S246
S348
Y200
Y22
T17
T186
T233
S239
β-Roll
β-Ladder
E
ZIKV NS2B-NS3 protease
S71
NS2B
NS3
F
ZIKV NS5
T292
Fingers
Mtase domain
RdRp domain
S663
S234
S237
Thumb

Figure 3

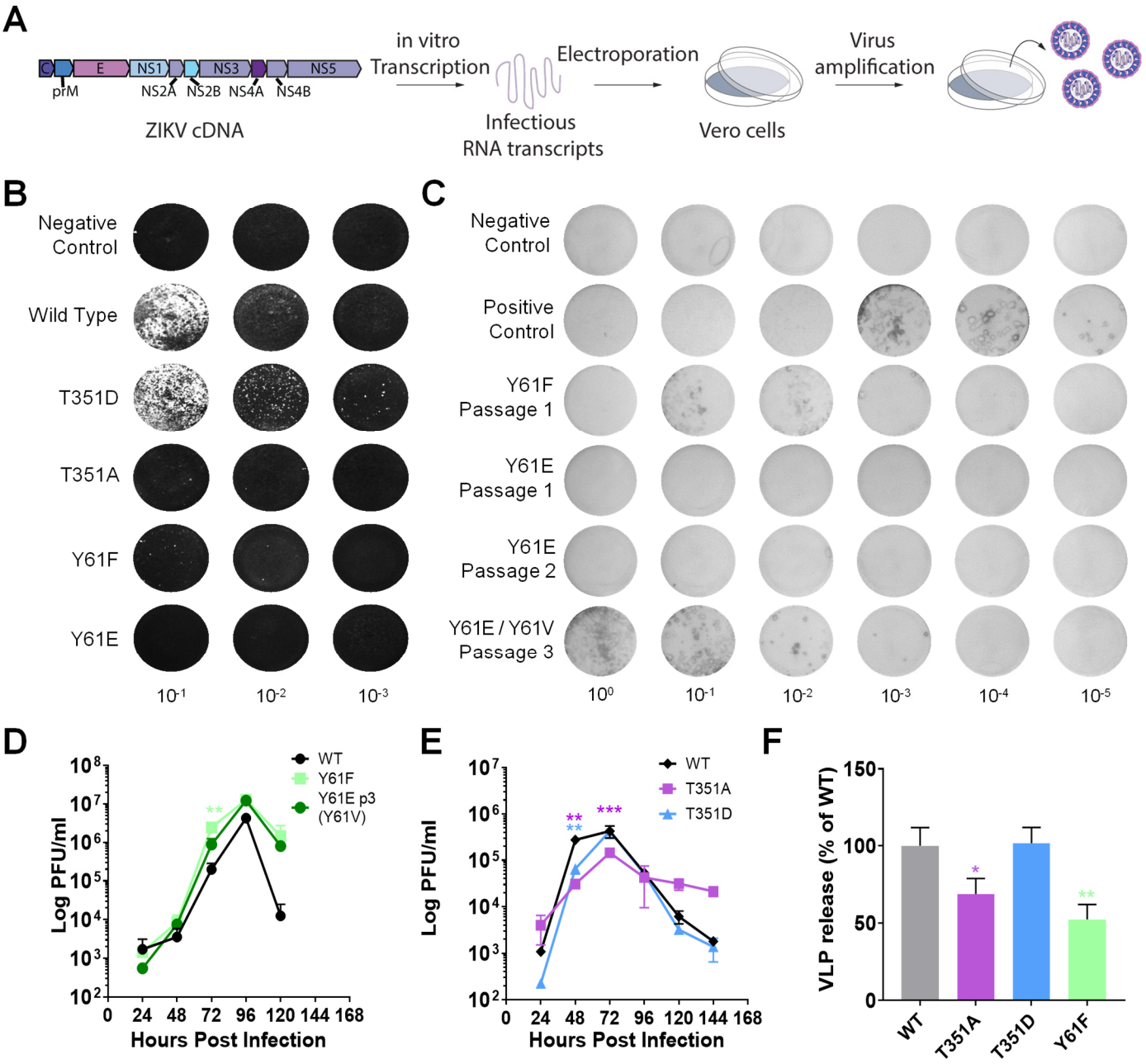
A
C
E
NS1
NS3
NS5
prM
NS2A
NS2B
NS4A
NS4B
ZIKV cDNA
in vitro Transcription
Infectious RNA transcripts
Electroporation
Vero cells
Virus amplification
B
Negative Control
Wild Type
T351D
T351A
Y61F
Y61E
10-1
10-2
10-3
C
Negative Control
Positive Control
Y61F Passage 1
Y61E Passage 1
Y61E Passage 2
Y61E / Y61V Passage 3
100
10-1
10-2
10-3
10-4
10-5
D
WT
Y61F
Y61E p3 (Y61V)
Log PFU/ml
Hours Post Infection
E
WT
T351A
T351D
Log PFU/ml
Hours Post Infection
F
VLP release (% of WT)
WT
T351A
T351D
Y61F

Figure 4

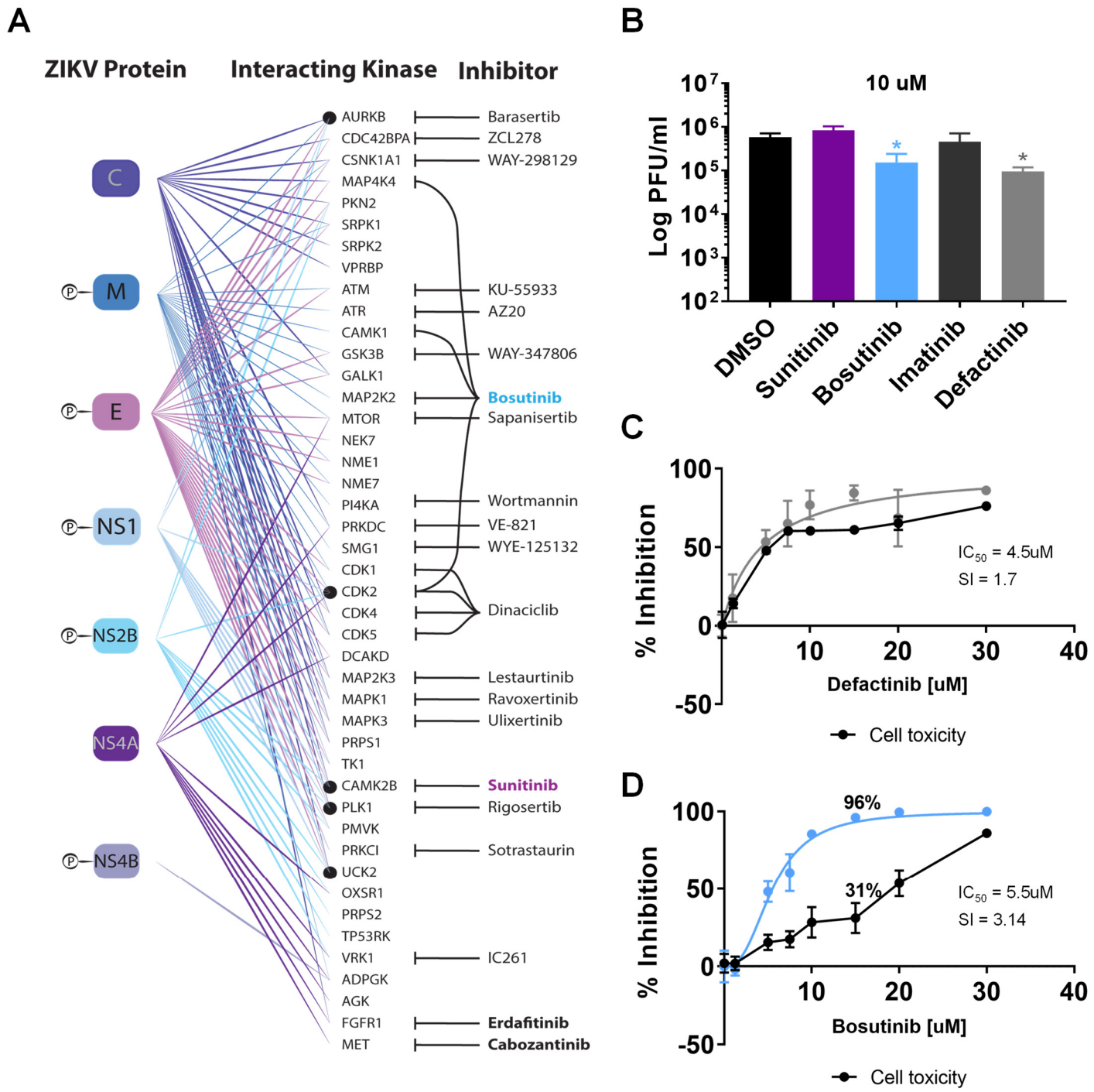
A
ZIKV Protein
Interacting Kinase
Inhibitor
C
M
E
NS1
NS2B
NS4A
NS4B
AURKB
CDC42BPA
CSNK1A1
MAP4K4
PKN2
SRPK1
SRPK2
VPRBP
ATM
ATR
CAMK1
GSK3B
GALK1
MAP2K2
MTOR
NEK7
NME1
NME7
PI4KA
PRKDC
SMG1
CDK1
CDK2
CDK4
CDK5
DCAKD
MAP2K3
MAPK1
MAPK3
PRPS1
TK1
CAMK2B
PLK1
PMVK
PRKCI
UCK2
OXSR1
PRPS2
TP53RK
VRK1
ADPGK
AGK
FGFR1
MET
Barasertib
ZCL278
WAY-298129
KU-55933
AZ20
WAY-347806
Bosutinib
Sapanisertib
Wortmannin
VE-821
WYE-125132
Dinaciclib
Lestaurtinib
Ravoxertinib
Ulixertinib
Sunitinib
Rigosertib
Sotrastaurin
IC261
Erdafitinib
Cabozantinib
B
10 uM
Log PFU/ml
DMSO
Sunitinib
Bosutinib
Imatinib
Defactinib
C
% Inhibition
Defactinib [uM]
IC50 = 4.5uM
SI = 1.7
Cell toxicity
D
96%
31%
% Inhibition
Bosutinib [uM]
IC50 = 5.5uM
SI = 3.14
Cell toxicity

Figure S1

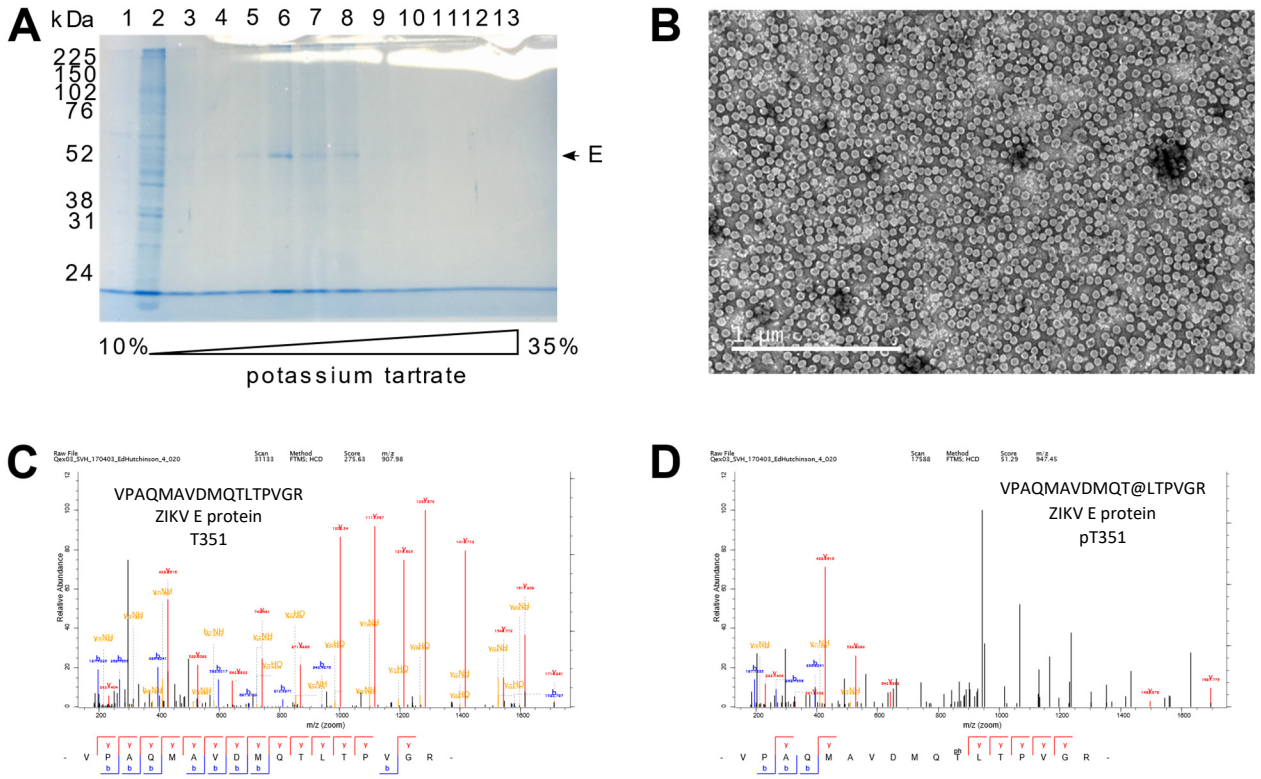
A
kDa
1 2 3 4 5 6 7 8 9 10 11 12 13
225
150
102
76
52
38
31
24
E
10%
35%
potassium tartrate
B
1 µm
C
VPAQMAVDMQTLTPVGR
ZIKV E protein
T351
Relative Abundance
m/z (zoom)
D
VPAQMAVDMQT@LTPVGR
ZIKV E protein
pT351
Relative Abundance
m/z (zoom)

Figure S2

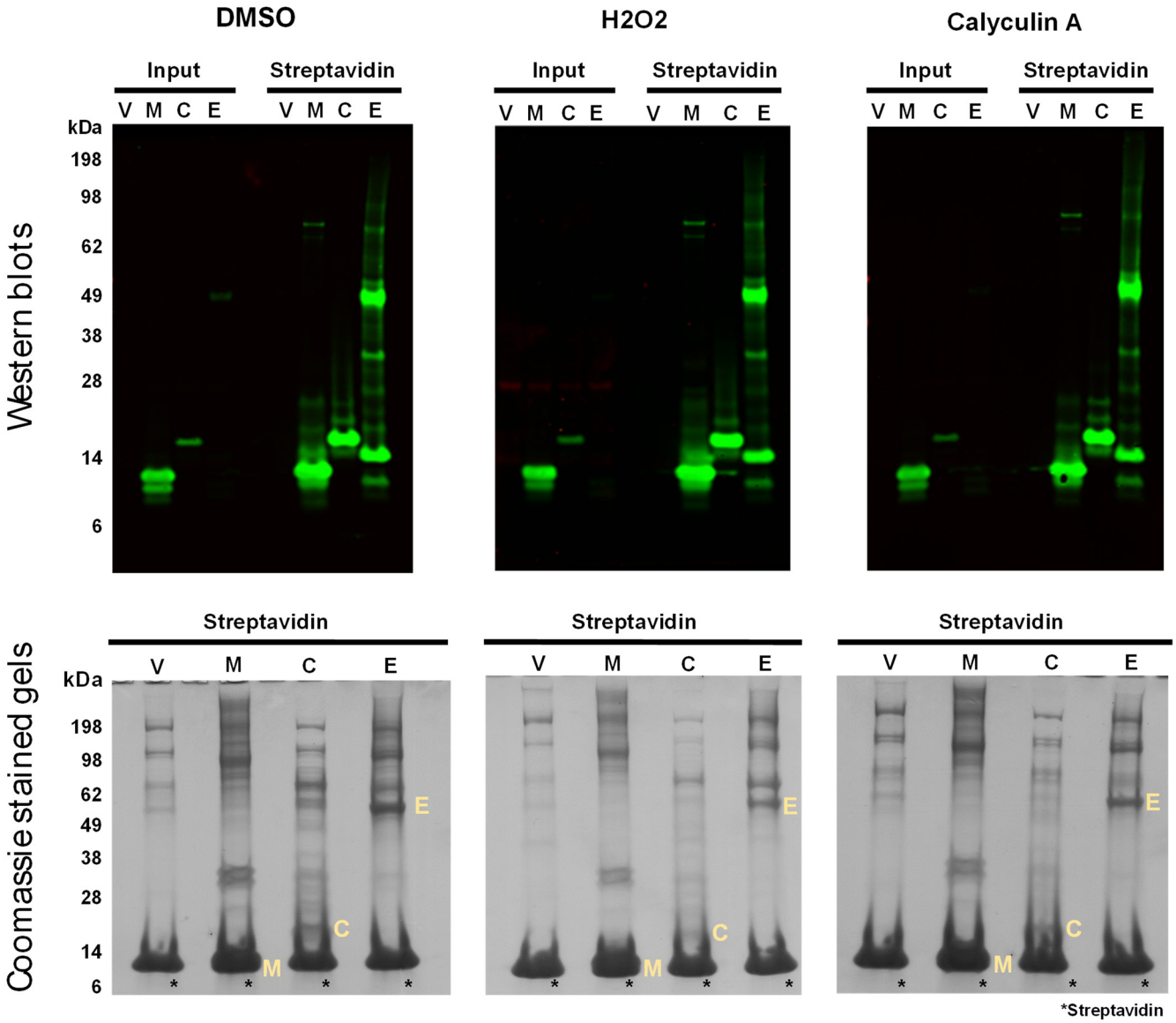
DMSO
H2O2
Calyculin A
Input
Streptavidin
V M C E
kDa
198
98
62
49
38
28
14
6
Western blots
Coomassie stained gels
E
C
M
*Streptavidin

Figure S3

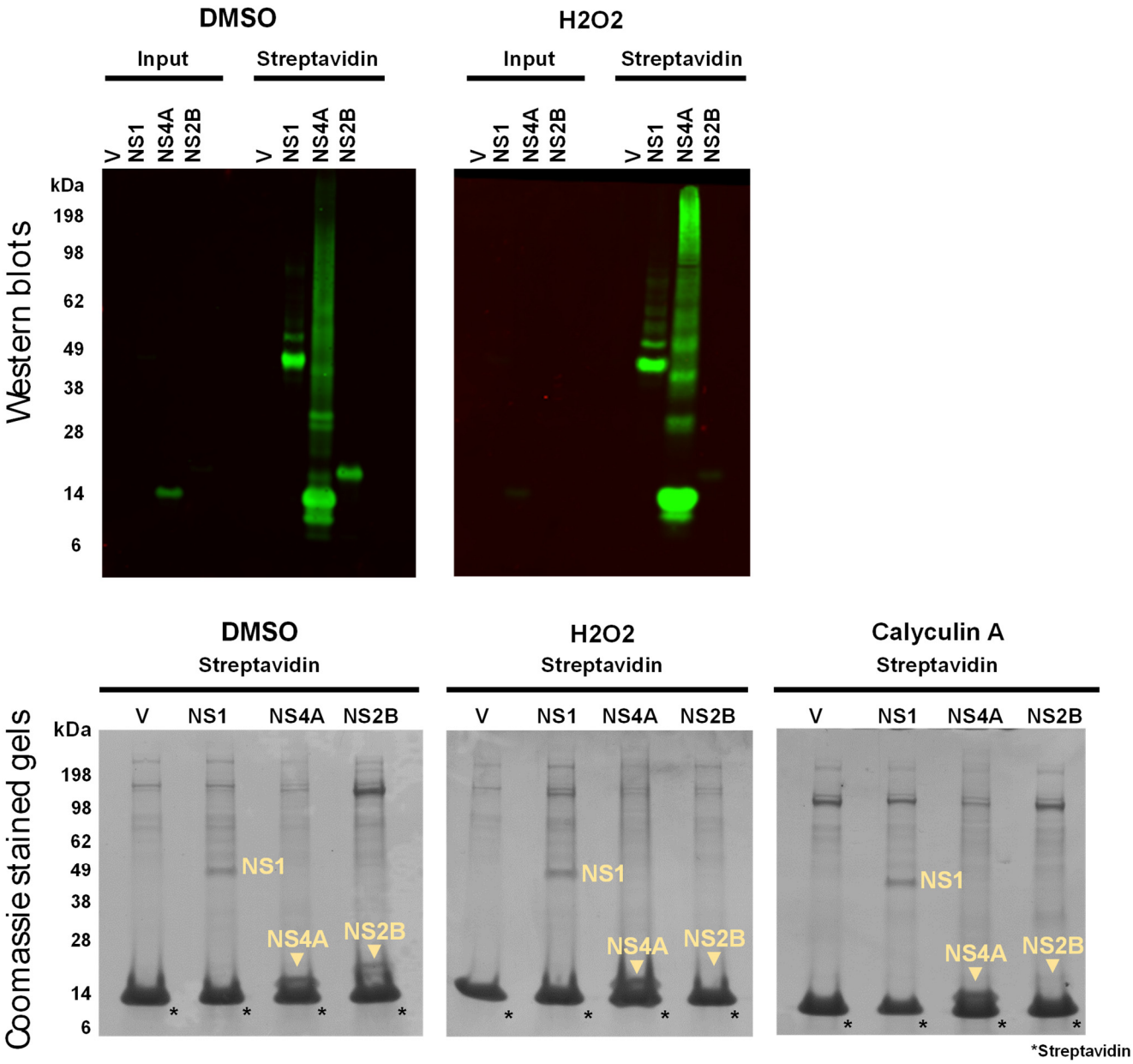
DMSO
H2O2
Input
Streptavidin
V
NS1
NS4A
NS2B
kDa
198
98
62
49
38
28
14
6
Western blots
Calyculin A
Coomassie stained gels
*Streptavidin

Figure S4

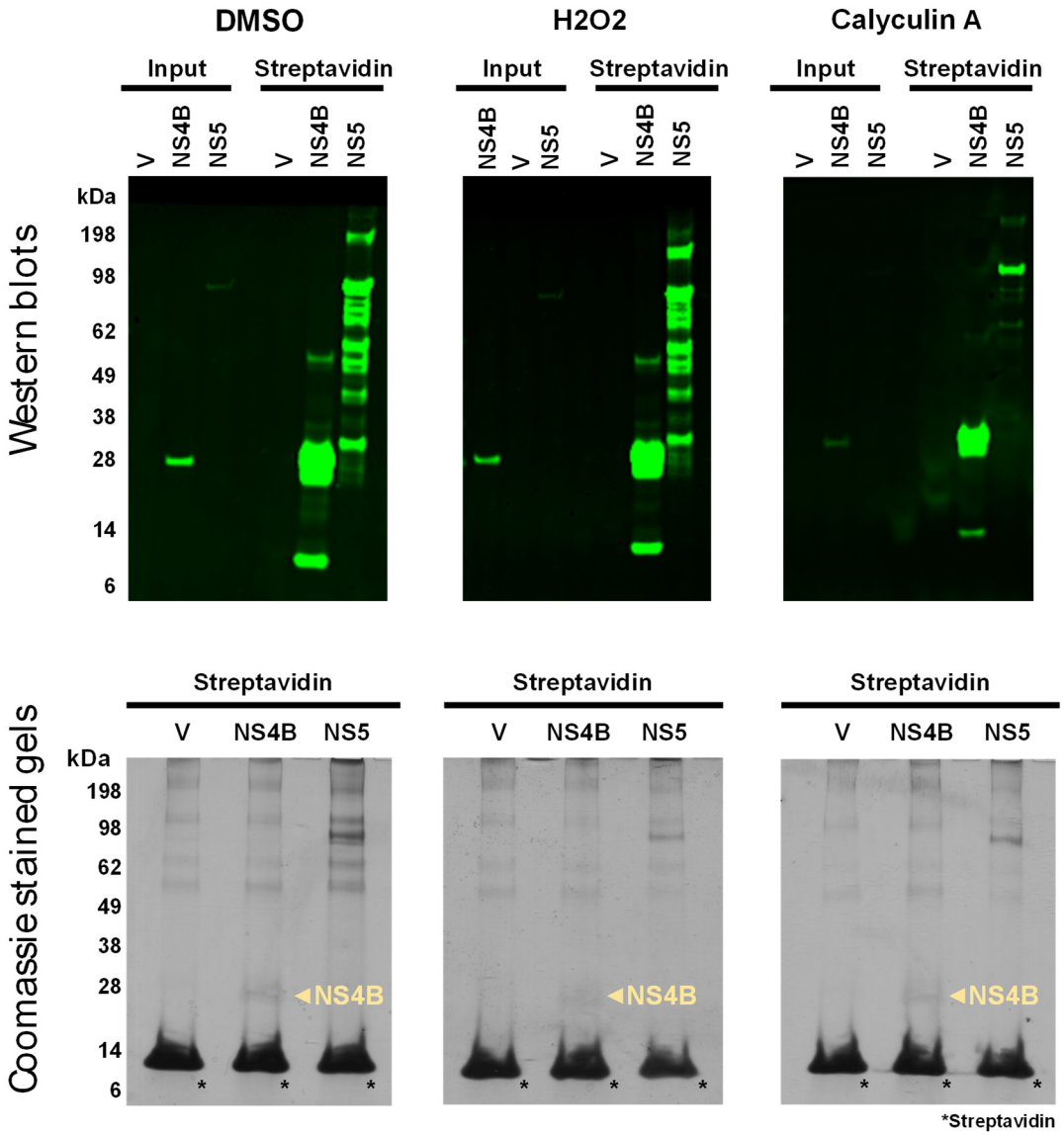
DMSO
H2O2
Calyculin A
Input
Streptavidin
V
NS4B
NS5
kDa
198
98
62
49
38
28
14
6
Western blots
Coomassie stained gels
◄NS4B
*Streptavidin

Figure S5

A

Positive Face – ZIKV E dimer

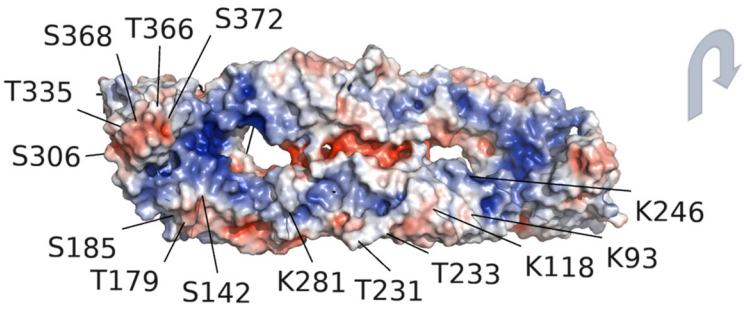

B

Negative Face – ZIKV E dimer

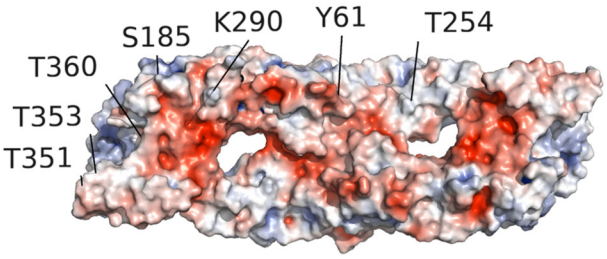

C

Neutral Border – ZIKV E dimer

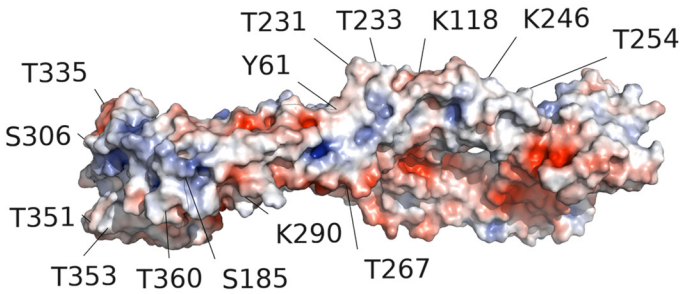

Figure S6

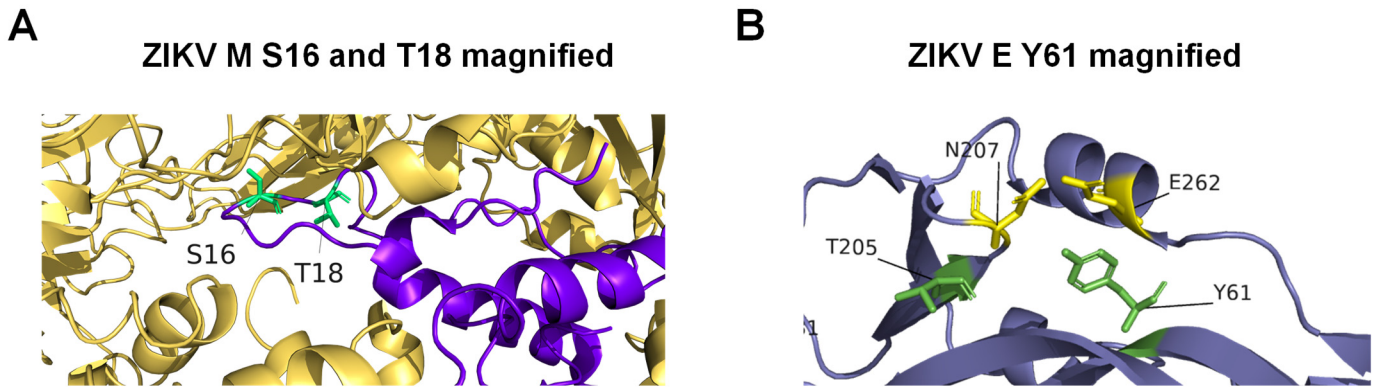
A
ZIKV M S16 and T18 magnified
S16
T18
B
ZIKV E Y61 magnified
N207
E262
T205
Y61

Figure S7

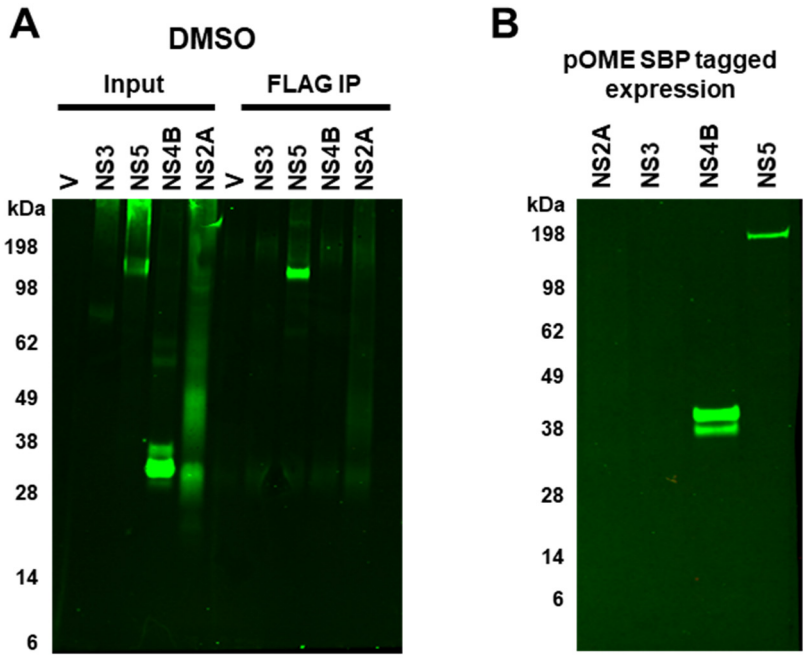
A
DMSO
Input
FLAG IP
V
NS3
NS5
NS4B
NS2A
V
NS3
NS5
NS4B
NS2A
kDa
198
98
62
49
38
28
14
6
B
pOME SBP tagged expression
NS2A
NS3
NS4B
NS5
kDa
198
98
62
49
38
28
14
6